MgAl and ZnAl layered double hydroxides modified with molybdate and tungstate anions as catalysts for oxidation of cyclohexane

Carolina Machado Terzi, Everton Henrique dos Santos, Charles Carvalho, Vanessa Prevot, Fernando Wypych, Claude Forano, Shirley Nakagaki

MgAl and ZnAl layered double hydroxides modified with molybdate and tungstate anions as catalysts for oxidation of cyclohexane

Carolina Machado Terzi[1,2], Everton Henrique dos Santos[1,3], Charles Carvalho[1,3], Vanessa Prevot[3], Fernando Wypych[2], Claude Forano[3]*, Shirley Nakagaki[1]*

[1]Laboratório de Bioinorgânica e Catálise, [2]Laboratório de Química de Materiais Avançados - [1,2,]Departamento de Química, Centro Politécnico, Universidade Federal do Paraná (UFPR) 81531990, Curitiba/PR, Brazil, [3]Université Clermont Auvergne, CNRS, INP Clermont, ICCF, F-63000 Clermont-Ferrand, France

*Corresponding authors: shirleyn@ufpr and claude.forano@uca.fr

Abstract

Catalytic oxidation of cyclohexane to cyclohexanol and cyclohexanone with H_2O_2 was performed at a mild temperature of 40 °C and atmospheric pressure, using ZnAl or MgAl layered double hydroxides (LDHs) **modified** with tungstate and molybdate anions as catalysts in heterogeneous medium. The catalysts were prepared by direct anion exchange reactions of tungstate and molybdate on LDHs intercalated with chloride/carbonate anions. All the solids showed catalytic activity in the cyclohexane oxidation, with slight selectivity for the ketone product. The catalytic efficiency was sensitive to the M^{2+} present in the composition of the LDH as well as to the anions. ZnAl-modified with WO_4 was more active and more selective for ketone than the MgAl-modified WO_4 or any molybdate-based LDH catalysts.

Keywords: molybdate, tungstate, cyclohexane oxidation, layered double hydroxides - LDHs, heterogeneous catalysis

Introduction

Selective oxidation of alkanes is a difficult reaction to perform, considering both kinetic and thermodynamic aspects [1,2]. Therefore, the oxo-functionalization process of these compounds, especially linear alkanes in their terminal position, has been intensely investigated, since the compounds resulting from this reaction have high value and are used in many areas of the chemical industry. For example, cyclohexane oxidation is one of the conventional methods to produce adipic

acid (AA), which is primarily used for the manufacture of nylon-6,6 polymer, in turn for production of polyurethanes as reactants to form plasticizers, lubricant components, polyester polyols, e-caprolactam, etc. Yearly global AA production is more than 3.5 million metric tons, with demand growth of 5% annually [3,4]. The abundance of alkanes derived from oil and the range of possible compounds resulting from their chemical transformations means that their oxo-functionalization is still widely investigated in catalytic processes. Hence, their use extends far beyond fuels [3–7].

Different catalytic approaches employing chemical compounds and enzymes have been investigated for development of efficient and selective alkane oxo-functionalization reactions. Related to enzymes, most metalloenzymes active for alkane oxo-functionalization use copper or iron as metal catalytic species, such as monooxygenase systems operating under mild physiological conditions. Inspired by these biological systems, different metal ion complexes, mainly Cu^{2+}, Fe^{3+}, Mn^{3+}, and Co^{3+}, have been investigated as biomimetic catalysts for oxo-functionalization of linear and cyclic alkanes [8–12]. Despite the promising results reported using, for example, metalloporphyrins [13–17], alkane oxo-functionalization remains a major catalytic challenge when aiming to scale up the results. Thus, the development of new technological processes to take advantage of these molecules is needed.

In addition to the cited metal compounds, tungsten and molybdenum compounds are have also been investigated as catalysts for this class of oxidation reactions, e.g., oxidation of alkanes, phenols, and olefins; alkene epoxidation; allylic acetoxylations to form glycerol from allylic alcohols; and asymmetric dihydroxylation of glutaraldehyde from cyclopentene [18–21]. These two metals are frequently used in different forms, like polyoxometalates (POM) [22-33], anions [34,35], complexes [36–40], in association with gold, platinum or copper nanoparticles [41–45], etc.

Regarding tungsten compounds, several WO_3 and tungstate-based catalysts have been found active for cyclohexene oxidation [41,46–50]. Sato et al. demonstrated the efficiency of Na_2WO_4 as a catalyst to convert cyclohexene to AA using 30% H_2O_2 in a biphasic system [46]. Also, Vafaeezadeh et al. demonstrated that silica-functionalized ammonium tungstate is a versatile oxidation catalyst for direct cyclohexene conversion into AA using H_2O_2[50]. Mai et al. [41] prepared a photothermal solid catalyst by loading Au nanoparticles (Au NPs) into WO_3 nanosheets (WO_3 NSs) to improve cyclohexane conversion and ketone-alcohol (KA) oil selectivity under solar light irradiation. High conversion of 9.0% and a high selectivity of 99.0% were observed, attributed to the improved light absorption, the effective charge separation, and the synergistic effect of photocatalysis and thermal catalysis.

Molybdenum species have also been investigated as catalysts for cycloalkane and cycloalkene oxidation reactions [32,33,51–55]. For instance, Conte et al. [32] prepared a molybdenum blue nanoring Mo^{5+}-O-Mo^{6+} (POM) and investigated it as a catalyst for solvent-free

cyclohexane oxidation to alcohol and ketone with O_2 gas. They observed a ketone/alcohol ratio (K/A) of 0.8 with 6% cycloalkane conversion to the products after 17 h of reaction. The strong catalytic activity was attributed mainly to the presence of Mo^{5+} species in the POM composition. Using MoO_3-containing MCM-41 mesoporous silica catalyst, Rana and Viswanathan [52] investigated the catalytic oxidation of cyclohexane into acetone, which led to a K/A ratio of 0.16 with up to 87.59% cyclohexanone selectivity while using 30 wt% H_2O_2. They attributed this result to the activity of tetrahedral MoO_4 sites in the solid structure. Also, using molybdenum and tungsten polyoxometalates supported on activated carbon fibers, Alcañiz-Monge et al. [33] investigated the influence of their respective peroxometallic intermediaries, formed *in situ* using hydrogen peroxide in acetonitrile, on the conversion of cyclohexane into adipic acid. They reported that compared to $[PW_{12}O_{40}]^{3-}$ catalytic species, the use of $[PMo_{12}O_{40}]^{3-}$-based heteropoly salts offered many advantages due to their stronger oxidizing power, presenting higher catalytic activity and higher selectivity to AA synthesis. Lastly, using the inexpensive catalyst ammonium molybdate ($(NH_4)_6Mo_7O_{24}$), Buonomenna and co-workers [55] reported the one-step cyclohexane oxidation to adipic acid using a microporous polymer membrane to compartmentalize the organic phase containing the substrate and the aqueous phase with the catalyst, hydrogen peroxide and succinic acid, to obtain selective oxidation of cyclohexane to adipic acid (90%).

Layered double hydroxides (LDHs) are a class of inorganic solids that can easily support polyoxometalate anions and can be designed as potential catalysts for oxidation reactions. LDHs consist of positively charged layers neutralized with exchangeable anions. The positive charges arise from the composition of LDHs based on metallic cations in different oxidation states (2+ and 3+) and M^{2+}:M^{3+} molar ratios. These positively charged layers are counterbalanced by hydrated or non-hydrated anions, located in the interlayer space and at the layer surface of the LDH. Due to the great flexibility of chemical composition of both the layers and the interlayer domains, which can accommodate different anions, this class of materials has been widely used for a variety of applications, among them catalysis [13, 15, 16, 56,57].

The catalytic properties of LDHs intercalated with tungstate and molybdate have been explored for various organic reactions such as olefin epoxidation [58,59], transesterification [60], H_2O_2-activated oxidation [61–64], alcohol dehydration [65] and oximation reaction [66]. Most of the Mo and W catalytic oxo species that have been immobilized in LDH matrices for oxidation reactions are tetrahedral anions (MoO_4^{2-} or WO_4^{2-}).

Concerning the oxygen species used for the catalytic oxidation reactions, in recent years the importance of hydrogen peroxide as an oxidizing agent has grown, because H_2O_2 is an environmentally friendly reactant, besides being cheaper and safer in comparison to other organic

peroxides, with a high effective-oxygen content (47%) [67], producing water as the resulting byproduct [2,6,67–70].

Tungstate and molybdate activation by H_2O_2 lead to the formation of active peroxo species $MO_2(OO)_2^{2-}$ according to **Equation 1**:

$$MO_4^{2-} + nH_2O_2 \Leftrightarrow MO_{4-n}(O_2)_n^{2-} + nH_2O \text{ (with M = Mo, W)} \qquad \textbf{Equation 1}$$

In appropriate pH conditions, tungstate or molybdate [71] can also promote the H_2O_2 disproportionation into a $^1O_2$ singlet (**Equation 2**):

$$2H_2O_2 \Leftrightarrow 2H_2O + {}^1O_2 \qquad \textbf{Equation 2}$$

LDHs modified with W and Mo polyoxometallates ($Mo_7O_{24}^{6-}$, $W_7O_{24}^{6-}$) have also been successfully evaluated as catalysts of alkene oxidation [62,63,72] and olefin epoxidation [58].

Intercalation of oxo- and polyoxotungstate and molybdate in LDHs is favored by their high negative charge density, even though some limitations arise due to the high affinity of LDHs toward competitive anions such as carbonate. Indeed, despite being known as anion exchangers, LDHs have an interaction affinity that depends on the chemical nature of the anions to be exchanged. The decreasing order of affinity can be exemplified as $CO_3^{2-} > SO_4^{2-} > OH^- > F^- > Cl^- > Br^- > NO_3^- > I^-$ [57].

In view of the known order of ionic affinity, LDHs have a higher affinity for carbonate ions (CO_3^{2-}) than for other ions, so it is more difficult to exchange these ions for others. However, for this class of material to be used as a platform capable of exchanging different ions with different functionalities, e.g., anions with catalytic properties, it is first necessary to deintercalate the carbonate ions without changing the crystallinity and/or size homogeneity of the layered particles [56,57,73,74].

Among the available methods to achieve this goal, the process based on controlled acidification of the reaction medium using a buffer solution of acetic acid/acetate in the excess presence of the anions, e.g., chloride ions, is suitable to promote the carbonate ion (CO_3^{2-}) exchange [73]. Based on this method, when the reaction medium is acidified, there is an increase in the amount of H^+ available in the solution, and these protons can react with the carbonate ions present in LDH, leading to the formation of hydrogen carbonate ions, which can again be protonated, leading to the formation of water and CO_2 which can finally be removed from the LDH.

Consequently, chloride Cl^- ions present in excess in the reaction medium are intercalated in the interlayer space. Since the chloride ion is a monovalent anion, the tendency to exchange this

anion for another of interest related to the carbonate anion is facilitated, especially if it has a greater number of charges.

In this work, we prepared and characterized new LDH-based catalysts, namely MAl-LDHs (M = Zn^{2+} or Mg^{2+}), exchanged with anionic molybdate or tungstate species, and compared their catalytic performances in the cyclohexane oxidation reaction with H_2O_2 to obtain cyclohexanone (K) and cyclohexanol (A) as main products (KA mixture).

Experimental

Synthesis of the catalysts

Preparation of the LDH precursors

MgAl-LDH (denoted MA) and ZnAl-LDH (denoted ZA) were prepared by co-precipitation of a solution of 200 mL containing 0.75 mol of $MgCl_2$ (for MA) or $ZnCl_2$ (for ZA) and 0.25 mol of $AlCl_3{\cdot}9H_2O$, with M^{2+}:Al^{3+} molar ratio of 3:1, according to a previously reported method [75]. The addition of the solution was performed under dynamic N_2 flow, constant magnetic stirring at room temperature and constant pH of 10.5, maintained by the addition of 2 mol L^{-1} NaOH solution for 6 hours. After the addition was completed, the dispersion was aged at 80 °C for 14 hours under dynamic N_2 flow and constant magnetic stirring. The white solid was separated by centrifugation, washed 3 times with deionized water and kept in dispersion for further use.

Preparation of the chloride-containing LDH

To prepare the LDH of ZnAl and MgAl intercalated solely with chloride (denoted by ZA-Cl or MA-Cl respectively), the carbonate intercalated ions were removed using the method described by Iyi et al. [73] under N_2 atmosphere and using decarbonated water. Then 100 mL of the ZA or MA dispersion was mixed with 100 mL of 2.5 mol L^{-1} NaCl solution and 100 mL of 0.1 mol L^{-1} buffer acetic acid/acetate solution. The dispersion pH was kept around 5.2 - 5.5 under magnetic stirring overnight at room temperature. The dispersion was centrifuged and the separated solid (ZA-Cl or MA-Cl) was washed with deionized and decarbonated water 3 times and kept in dispersion for further use.

Preparation of the LDH modified with molybdate and tungstate anions

Molybdate and tungstate exchanged ZA-Cl or MA-Cl (denoted as ZA-W, ZA-Mo, MA-W or MA-Mo) were obtained by direct surface ion-exchange reactions of ZA-Cl or MA-Cl with $Na_2WO_4{\cdot}2H_2O$ or $Na_2MoO_4{\cdot}2H_2O$ [69]. To prepare the LDH-W samples, ZA-Cl or MA-Cl (5 g) was dispersed in 50 mL of decarbonated water previously purged with N_2 and the pH was adjusted to 9.5 by the addition of 0.1

mol L^{-1} NaOH solution. The dispersion was magnetically stirred at room temperature under N_2 flow and then a decarbonated water solution of $Na_2WO_4 \cdot 2H_2O$ (100 mL, 0.1 mol L^{-1}) was slowly added during 3 hours.

To complete the reaction, the mixture was maintained at 80 °C under dynamic N_2 flow for 16 h. The resulting products were filtered, washed thoroughly with deionized and decarbonated water, and dried for 14 h at 50 °C. A similar procedure was used to prepare ZA-Mo and MA-Mo using $Na_2MoO_4 \cdot 2H_2O$ decarbonated water solution (0.1 mol L^{-1}).

Oxidation of cyclohexane

ZA-W, ZA-Mo, MA-W and MA-Mo were investigated as catalysts for cyclohexane oxidation using hydrogen peroxide [69]. In the procedure for cyclohexane oxidation, the catalytic experiments were carried out at atmospheric pressure in a glass vial batch reactor (10 mL), equipped with a magnetic stirrer in dark conditions using a cyclohexane:H_2O_2 molar ratio of 1:5. In a typical run, about 50 mg of the catalyst (ZA-W, ZA-Mo, MA-W, MA-Mo) was dispersed with 5.0 mL of acetonitrile solvent in a vial reactor under stirring and cyclohexane (1 mmol) and 35% H_2O_2 aqueous solution (5 mmol) was added. The reaction medium was magnetically stirred for 3 h at 40 °C. The catalysts were separated by centrifugation (4000 RPM) and washed with 3 portions of 1.0 mL of acetonitrile. The supernatant and the washing solutions were transferred to the same 10 mL volumetric flask and analyzed with an Agilent 6850 gas chromatograph (flame ionization detector) equipped with a 30 m long DB-WAX capillary column with 0.25 mm internal diameter (J&W Scientific), using n-octanol as internal standard. Control experiments (blanks) were carried out by mixing the reactants (substrate and H_2O_2) without any catalyst and also in the presence of **i)** tungstate- or molybdate-free LDH (ZA-Cl or MA-Cl) or **ii)** sodium tungstate or sodium molybdate salts. The H_2O_2 concentration was measured by standard iodometric titration. In addition to these general reaction conditions, reactions were also carried out at different reaction times and amounts of catalysts to achieve optimized conditions to maximize the desired products. The modified reaction conditions were reaction time (3 h, 8 h, 16 h, and 23 h), and amount of catalyst (50 mg and 15 mg). The reactions were performed in duplicate or triplicate and the conversion percentage yield of cyclohexane to the alcohol cyclohexanol (A) and ketone cyclohexane (K) products obtained (Table 3) was based on the amount of cyclohexane (substrate) added, with an estimated error between 3 and 10%.

Materials characterization

Fourier-transform infrared spectroscopy (FTIR) measurements were carried out using a Thermo Nicolet 5700 spectrometer, employing KBr pellets at a mass ratio of 1:100 (sample :KBr) with resolution of 4 cm^{-1} and accumulation of 64 scans.

The Raman spectra were recorded from 150 to 1500 cm^{-1} at room temperature using a confocal micro-Raman spectrometer (Jobin Yvon T64000) with an excitation wavelength of 514.5 nm (argon-ion laser-line). Spectra were acquired with resolution of 1 cm^{-1} with a charge coupled device (CCD) multichannel detector cooled by liquid N_2 coupled to an Olympus confocal microscope. Zeta potential data were acquired with a Nanosizer ZS from Malvern Instruments equipped with a 633 nm He-Ne laser with non-invasive back scattering (NIBS) configuration (173°). For analysis, solids were dispersed in deionized water at a concentration of 0.01% (w/w).

For the X-ray diffraction (XRD) analysis, the solids were placed on glass sample holders and the measurements were performed in reflection mode using a Shimadzu XRD-6000 diffractometer operating at 30 kV and 40 mA (Cu Kα radiation λ = 1.5418 Å) with Bragg-Brentano θ-2θ geometry with a scan rate of $1°\cdot min^{-1}$.

Transmission electron microscopy (TEM) and selected area electron diffraction (SAED) measurements were performed with a JEOL JEM-1200 microscope operating at 110 kV. The samples were dispersed in propanone and deposited on FCF300-CU grids (300 mesh) covered with formvar/carbon film.

Scanning electron microscopic images (SEM) and energy dispersive spectra (EDS) were obtained with a Tescan VEGA3 LMU device, using tension of 10 KV. The samples were deposited on aluminum stubs and the EDS spectra were collected with an SDD detector with 80 mm^2 in the range of 0 to 10 KeV. Then the samples were gold-sputtered to obtain the SEM images.

The UV-Vis spectra of the solid samples were obtained using a Varian Cary 100 BIO Uv-visible spectrophotometer by placing the samples in a Teflon sample holder and measuring the absorbance in the 200 to 800 nm range.

The textural properties were determined with a NOVA 1000 analyzer (Quantachrome) after degasifying the samples under vacuum for 6 hours (ZnAl samples were maintained at 150 °C during this period and those of MgAl at 90 °C). The adsorption/desorption isotherms for N_2 were obtained in a relative pressure range from 0.05 to 0.99, and the specific surface area was calculated using the multi-point Brunauer-Emmet-Teller method (B.E.T.), with a relative pressure range from 0.05 to 0.3.

Results and discussion

Due to the strong ionic affinity of carbonate for LDH layers, to obtain LDH solids with surface modified by tungstate and molybdate anions, two-step synthesis was performed involving first the coprecipitation of ZnAl and MgAl LDH containing chloride (ZA and MA respectively) followed by a harsh acidic treatment to fully exchange the undesirable carbonate anions of the precipitated solids (ZA-Cl and MA-Cl respectively) [56,57,73].

Figure 1 shows the X-ray powder diffraction patterns of the LDH precursors (ZA and MA) (Fig. 1A, C) in addition to the chloride LDH prepared after the decarbonation treatment (ZA-Cl and MA-Cl) (Fig. 1B, D).

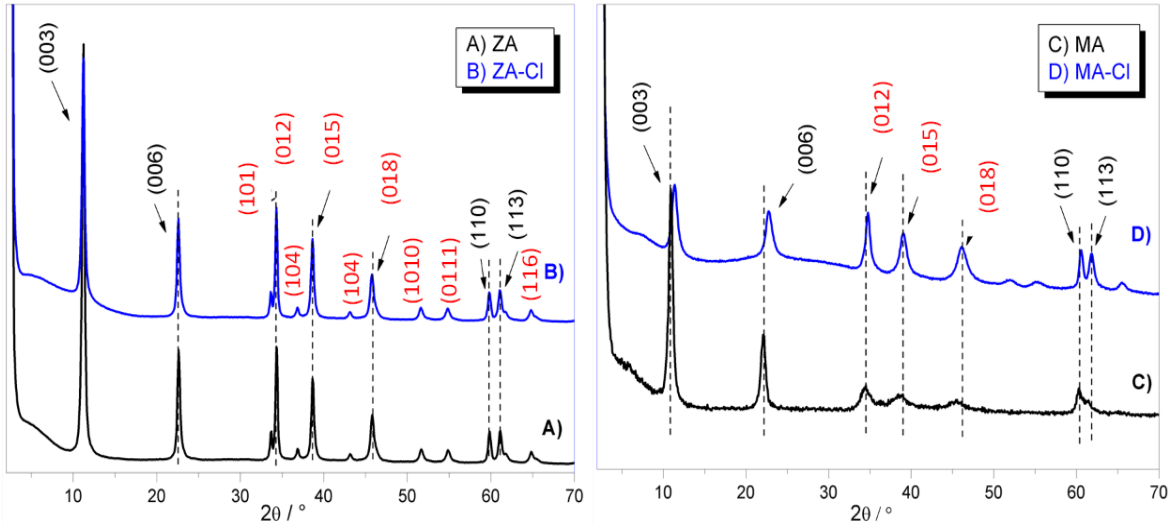

Figure 1. X-ray powder diffraction patterns of synthesized LDH solids before (A for solid **ZA** and C for solid **MA**) and after (B for solid **ZA-Cl** and D for solid **MA-Cl**) the carbonate deintercalation process.

All four samples displayed (Fig. 1) diffraction patterns typical of LDH structures (hexagonal lattice with rhombohedral R-3m symmetry), with well defined (hkl) diffraction peaks. The basal harmonic diffraction peak series occurred at low angles (003, 006), corresponding to the diffraction by atomic planes parallel to the layers, while the (110) diffraction peak in the 60° region indicates the metal-metal distance and allows calculating the cell parameter ($a = 2d_{110}$) [76]. Analysis of the ZnAl-LDH diffraction patterns (Fig. 1A, B) revealed practically no difference between the diffraction profiles before (Fig. 1A) and after the carbonate removal (Fig. 1B). The basal distances calculated using Bragg's equation, of both LDH ZA and ZA-Cl, were similar (d = 7.8 Å). These distances correspond to LDH gallery expansion due to Cl^- anion (r_i = 181 pm) intercalation, as reported for chloride LDH [57,77,78]. Indeed, both ZA and ZA-Cl LDH phases contain low carbonate anion contents as confirm by FTIR analysis (Fig. 3). Obviously, precipitation condition under

drastic N_2 gas flow, already prevented the formation of undesired LDH-CO_3 as the major phase, and further decarbonation process (step 2) did not improve much CO_3^{2-} decontamination. Based on XRD data and FTIR, it is difficult to infer with certainty whether part of carbonate anions were co-intercalated with Cl^- anion rather than totally adsorbed at the surface.

MA-Cl LDH displayed lower crystallinity (broader full width at half maximum (FWHM) of hkl diffraction lines) than ZnA-Cl LDH (Fig. 1C, D), as often observed. The carbonate removal process leads to XRD patterns with increased diffraction line widths (Fig. 1D), particularly visible for the (110)/(113) doublet, suggesting a decrease of both crystallinity and ordered domain size. Regarding the (003) and (006) peaks positions, slight shifts toward higher 2θ values were observed after the carbonate deintercalation/exchange process, indicating a decrease of the basal distance from 8.0 Å for MA to 7.7 Å for MA-Cl (Fig. 1D). This can be explained by the removal of co-intercalated CO_3^{2-} anions that leads to a pure MA-Cl phase with the typical interlayer distance of 7.7 Å.

Samples prepared by anion exchange of molybdate (Fig. 2B, F) and tungstate (Fig. 2C, E) anions displayed XRD patterns with similar diffraction line series, suggesting these reactions occurred retaining the LDH structure. No basal distance change was observed after the molybdate and tungstate exchange reaction, suggesting that intercalations were not obtained (Fig. 2A, B, C). The basal distances of 7.8 Å were compatible with the presence of either carbonate or chloride ions intercalated between the layers. Moreover, after MoO_4^{2-} and WO_4^{2-} exchange, the LDH XRD patterns (Fig. 2E, F) showed a drastic decrease in intensity of the basal peaks, especially for the MA samples, indicating that crystallinity seemed to be mainly impacted by this process. This is typical of a loss of layer stacking order.

The question of whether molybdate and tungstate were adsorbed at the surface of the layers or intercalated between the LDH layers remains. Many publications [64,65,79] dealing with the intercalation of MoO_4^{2-} and WO_4^{2-} in LDHs under reaction conditions similar to those used in this work (basic pH and thermal activation) have reported basal distances around 7.9 Å. However, MoO_4^{2-} and WO_4^{2-} entities with respectively metal-O distance W-O = 1.78-1.79 Å and Mo-O = 1.75-1.78 Å, displayed thermochemical radii greater than SO_4^{2-} anion radius (S-O distances 1.47-1.49 Å) and should lead, after intercalation in LDH, to a greater structural expansion of dehydrated sulfate (8.9 Å) [80,81]. Even though well crystalized, LDH-MoO_4^{2-} and LDH-WO_4^{2-} have not yet been synthesized. Only a few publications have mentioned an increase of basal distance after molybdate and tungstate intercalation. Mohapatra et al. [82] mentioned values of 8.59 Å and 9.11 Å for Zn_3Y- WO_4^{2-} and Zn_3Y-MoO_4^{2-} respectively. Similar basal spacing was obtained for Zn_2Cr-WO_4 (9.15 Å) [83]. These structural data are consistent with oxometallate anions and water molecules that are densely packed in the

LDH galleries. Hence, accessibility to catalytic intercalated species with such a non-porous compact structure is questionable in terms of kinetic and efficiency reactivity or economic cost.

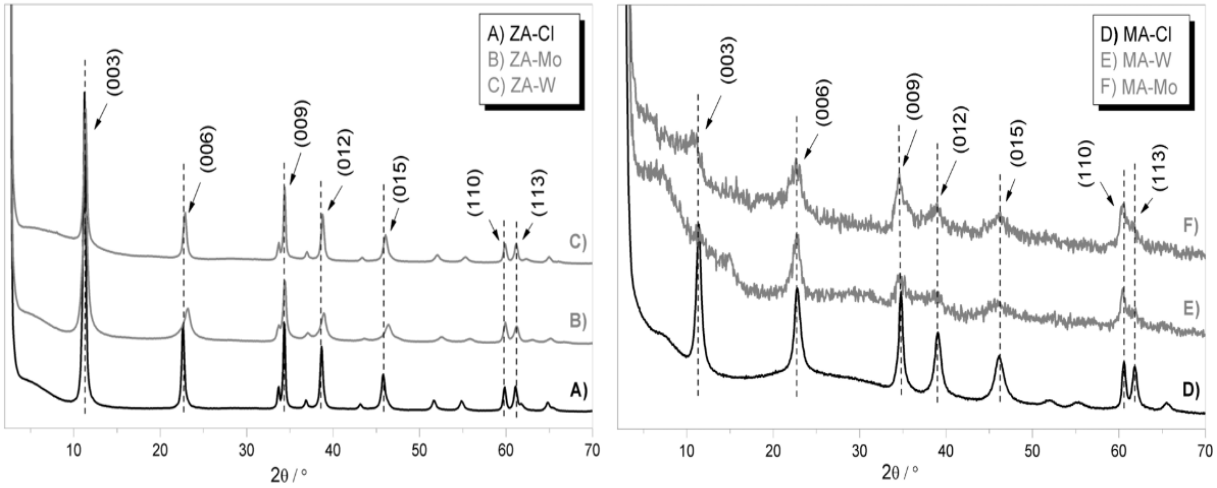

Figure 2. Powder X-ray diffraction patterns of LDHs before (A and D) and after tungstate (C and E) and molybdate (B and F) reactions. Here this figure is confusing. Left, blue is molybdate, with is tungstate. The same for red colored patterns. Better to keep the same colors. To be in accordance with fig. 3, just change fig. 2, left side.

The semi-quantitative chemical compositions of the various materials were obtained from EDS analysis. First of all, the atomic composition determined by EDS for MA-W, MA-Mo, ZA-W and ZA-Mo LDH samples (Table 1) corresponded to high content values of molybdate and tungstate anions loaded in LDHs. The experimental Mg^{2+}/Al^{3+} molar ratio of MA samples (2.84 – 2.88) were close to the one (3.0) initially fixed in the preparation procedure. Subsequent coprecipitation, decarbonatation and oxometallate reactions did not modify the Mg^{2+}/Al^{3+} chemical composition of the layers. Differently, the ZA solids displayed Zn^{2+}/Al^{3+} molar ratio (1.86 - 1.93) near 2.1 instead of the 3.1 imposed during coprecipitation. Obviously, under coprecipitation ZnA, LDHs reached the most stable composition of Zn_2A, with the best ordered structure, as shown by the XRD patterns. Similarly, after the exchange reactions with MoO_4^{2} and WO_4^{2-} on ZA-Cl and MA-Cl, the LDHs retained the M^{2+}/M^{3+} ratio of their precursors. From the data of Table 1, it is clear that molybdate and tungstate were not fully exchanged in LDH even though chloride anions were removed (except for ZA-W). The maximum percentage of anion exchange capacity (AEC) was reached for ZA-Mo (68%). Competition of even traces of carbonate prevents the preparation of pure LDH-MoO_4 and LDH-WO_4 phases. Obviously, diffusion of oxometallate in the LDH bulk is probably structurally restricted, favoring the intercalation of CO_3^{2-} anions in the interlayer spaces, while molybdate and tungstate

covered the platelet-like particles' surface. Nevertheless, the contents of catalytic species on the surface were high, between $9.65x10^{-4}$ and $1.10x10^{-3}$ mol g^{-1}.

Table 1. M^{2+}/M^{3+}/anion atomic ratio calculated based on EDS results.

LDH	Zn^{2+}/Al^{3+} or Mg^{2+}/Al^{3+}	MoO_4^{2-}or WO_4^{2-}/Al^{3+} (% of AEC)#	Cl^-/Al^{3+}	CO_3^{2-}/Al^{3+} *	Σ anions/Al^{3+}	Calculated loading values (mol·g^{-1})
ZA-Cl	1.86	0.00	0.64	0.18	1	-
ZA-Mo	1.93	0.34(68%)	0.00	0.16	1	$1.13x10^{-3}$
ZA-W	1.91	0.27 (54%)	0.16	0.15	1	$9.45x10^{-4}$
MA-Cl	2.84	0.00	0.78	0.11	1	-
MA-Mo	2.87	0.28 (56%)	0.00	0.22	1	$9.65x10^{-4}$
MA-W	2.88	0.12 (24%)	0.00	0.38	1	$1.10x10^{-3}$

*CO_3^{2-} was obtained from calculation based on electroneutrality of the overall LDH structure. #Anion exchange capacity (AEC). Novamente ZA e MA, não seria ZA-Cl e MA-Cl? Está confuso no texto todo.

TGA analyses (Fig. SI-1) confirmed the change in composition after oxometallate loading and the effect of the oxyanions on the thermal decomposition profile. Carbonate decomposition is associated with the thermal events around 410 – 420 °C, but it may last up to 900 °C when CO_3^{2-} anions are trapped in the collapsed layered double oxide structure (MA and ZA), which was clearly and surprisingly not the case for LDHs loaded with molybdate and tungstate. As evaluated from the mass loss of the intermediate thermal event (410 – 420 °C), MgAl LDH had higher carbonate contents than ZnAl LDH (Table1). This can be explained by the higher basicity of the MgAl LDH compared to ZnAl.

FTIR and Raman spectra confirmed that both oxometallate MO_4^{2-} (M= Mo, W) and carbonate CO_3^{2-} anions coexist in the ZA and MA LDH structures. The ν_3 asymmetric and ν_1 symmetric stretching vibration modes at around 1365 and 1060 cm^{-1}, respectively, of the intercalated carbonate are observed in all FTIR spectra (Fig. 3) [84]. The intensity of these bands slightly increased after oxometallate exchange. The ν_1 mode at 1065 cm^{-1} was also active in the Raman spectra, but the low intensity of the corresponding bands confirmed the small content (Fig. 4). Also, the infrared spectrum of ZA-Cl clearly evidenced that if carbonate anions were present, either intercalated or adsorbed at the surface, the fraction was minor (Fig. 3).

The low energy absorption domains were characteristic of the LDH layers [85] with M-OH vibration modes at 735 and 675 cm^{-1} for MA species [86,87] and at 660 and 591 cm^{-1} for ZA species [88,89]. Lattice vibrations (O-M-O and MO_6 vibrations) appeared as two bands in the Raman spectra, at 489 and 548 cm^{-1} for ZnAl LDH and 471 and 553 for cm^{-1} MgAl LDH.

MoO_4^{2-} and WO_4^{2-} containing LDH displayed typical oxometallate tetrahedral vibration modes. For the molybdate modified LDHs, ν_3 asymmetric Mo-O bond stretching modes were observed at 806 and 831 cm^{-1} respectively for MA-Mo and ZA-Mo, while the ν_1 Mo-O symmetric stretching band was only visible for ZA-Mo. ν_4 asymmetric bending modes, expected around 550 and 510 cm^{-1} , were superimposed with the LDH lattice vibrations [5,90–92].

MA-W and ZA-W showed typical bands related to ν_1 symmetric W-O stretching modes at 924 (MA-W) and 914 cm^{-1} (ZA-W) [92], and the W-O ν_3 stretching modes at 630 cm^{-1} of MA-W, while at 738 and 674 cm^{-1} they referred to ZA-W .The bands attributed to ν_4 asymmetric bending modes are expected under 425 cm^{-1} for W-O and therefore were not observed in the utilized spectral range [92,93].

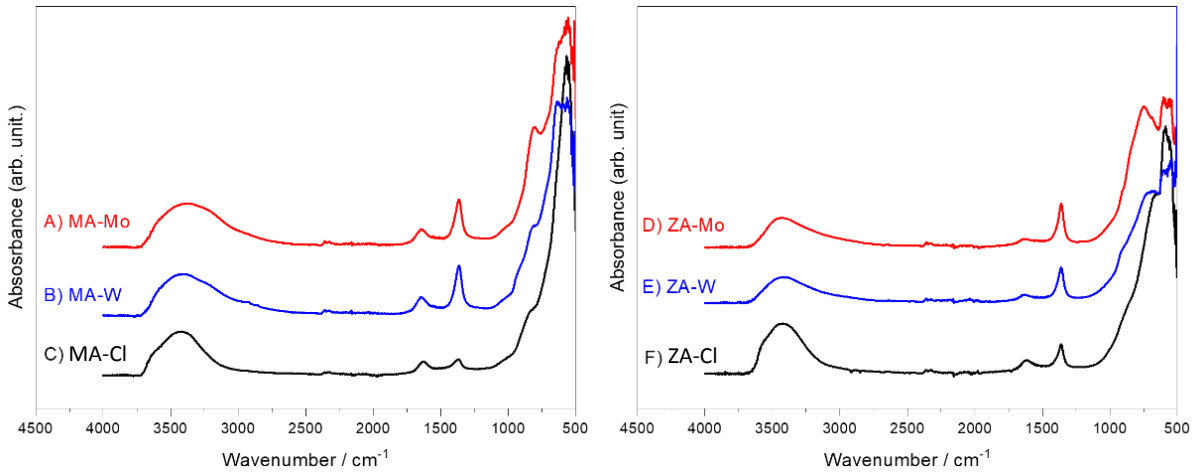

Figure 3. FTIR vibrational spectra of the prepared solids: A, B and C for MA-Mo, MA-W and MA-Cl; and D, E and F for ZA-Mo, ZA-W and ZA-Cl, respectively.

For tetrahedral (Td) MO_4 species, the four vibration modes ($\nu_1(A_1)$, $\nu_2(E)$, $\nu_3(F_2)$, $\nu_4(F_2)$) were all Raman active. The Raman spectra of LDH-MoO_4 (Fig. 4C, F) showed an intense band in the region of 900-913 cm^{-1} (900 and 913 cm^{-1} for MA-Mo and ZA-Mo respectively). We attributed this band to the ν_1 symmetric stretching mode of Td MoO_4. Furthermore, there was a lower intensity band in the region of 323 cm^{-1}, which could correspond to either the $\nu_2(E)$ or $\nu_4(F_2)$ angular deformations. These results were similar to data reported in the literature (897 and 317 cm^{-1}) [94]. In the MA-Mo spectrum, a shoulder band appeared at 944 cm^{-1}, which could be attributed to the presence of heptamolybdate ($Mo_7O_{24}^{6-}$) species, suggesting that this solid is composed by a mixture between molybdate and heptamolybdate ions [68,95].

The Raman spectra of WO_4^{2-} containing LDH (Fig. 4B for ZA-W and Fig. 4E for MA-W) were very similar to those of LDH-MoO_4^{2-}, with ν_1 and ν_3 modes appearing at 935 cm^{-1} and 355 cm^{-1}. The

broad shoulder at 830 cm^{-1} probably arose from the splitting of the ν_3(F2) vibration due to reduction of symmetry from the cubic point Td symmetry to lower symmetry when WO_4^{2-} attached to the LDH surface [96]. Such broad bands were also observed for MoO_4 loaded samples. Like the bands of the WO_4^{2-} anions, there was also a shoulder in the region of 966 cm^{-1}, which can be attributed to the presence of heptatungstate ($W_7O_{24}^{6-}$) ions, suggesting that the solid MA-W can also be composed of a mixture of tungstate and heptatungstate ions [97].

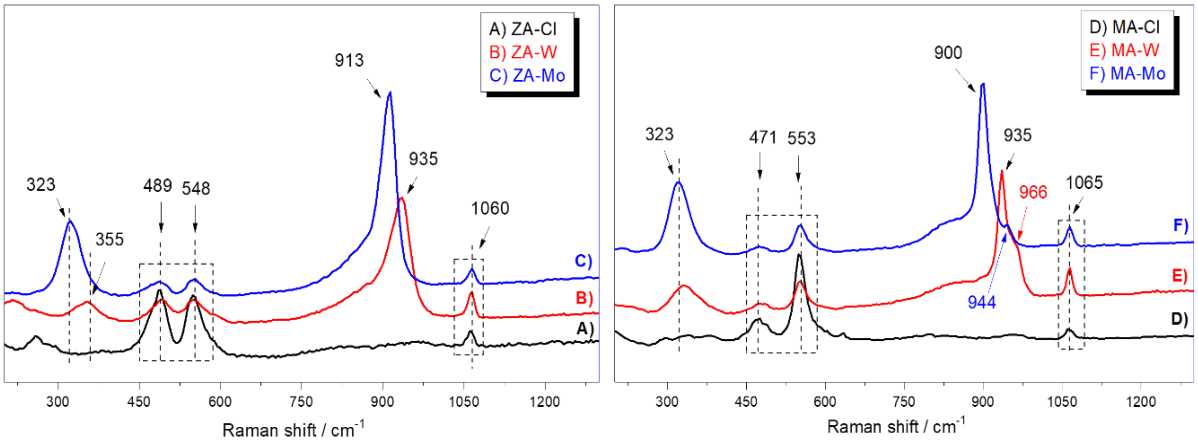

Figure 4. Raman vibrational spectra of the prepared solids before the ion exchange process (A: solid ZA-Cl and D: solid MA-Cl); and after the exchange of chloride ions by molybdate or tungstate ions (B: solid ZA-W, C: solid ZA-Mo, E: solid MA-W and F: solid MA-Mo).

While exchange reactions were performed at basic pH (9.5) to ensure adsorption of tetrahedral MO_4^{2-} species, the LDH surface can have a slightly less acidic environment, which shifts the speciation equilibrium to partial formation of polyoxometalate species, namely heptamolybdate ($Mo_7O_{24}^{6-}$) and heptatungstate ($W_7O_{24}^{6-}$), as observed in the Raman spectra for MA-Mo and MA-W. To better identify the nature and the proportion of the immobilized oxometallate species on the solids MA and ZA, diffuse reflectance UV-Vis spectra were acquired to quantify the oxometallate species' proportion (Fig. 5).

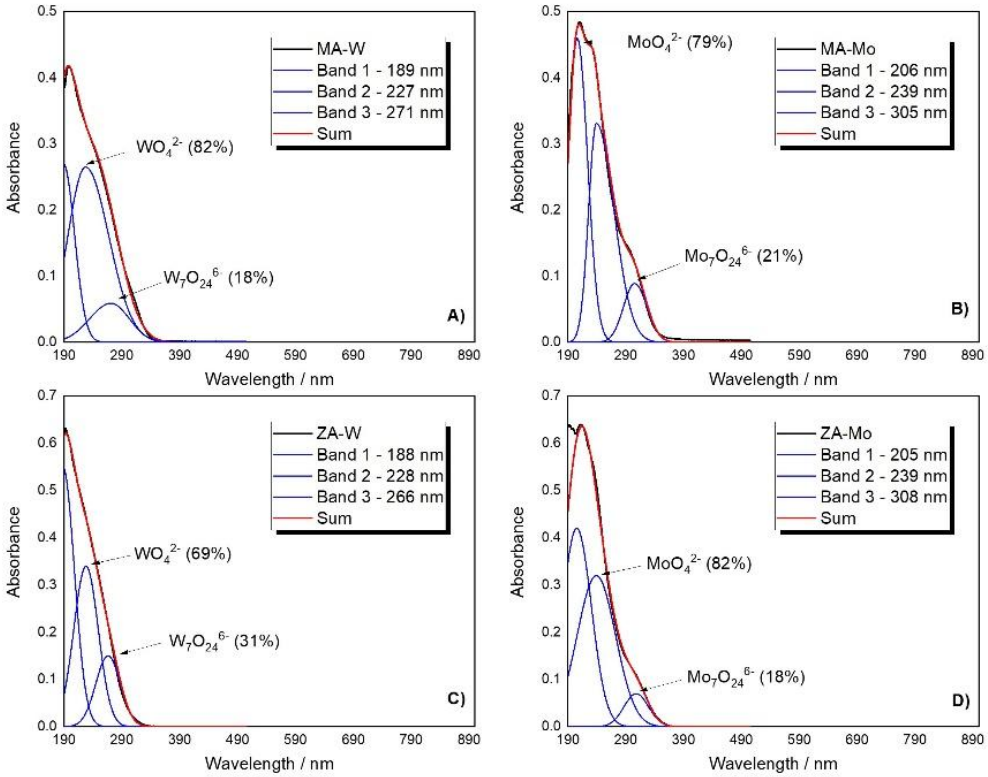

Figure 5. Experimental UV-Vis electronic spectra of solids MA-W (A), MA-Mo (B), ZA-W (C) and ZA-Mo (D) (black line) and their respective deconvolution substances (blue and red lines) with regard to the main species tungstate (WO_4^{2-}), heptatungstate ($W_7O_{24}^{6-}$), molybdate (MoO_4^{2-}) and heptamolybdate ($Mo_7O_{24}^{6-}$).

The experimental spectra were deconvoluted in Gaussian curves while the ratio between the anionic species' typical bands was estimated in percentage, considering the areas of the bands resulting from the deconvolution process. Data are reported in Table 2. For comparison, the loading value of the tungstate or molybdate species (mol) in the mass of the solid MA or ZA (mol/g) were also estimated.

Table 2. Estimated loading of oxometallate species in the LDHs samples according to UV-Vis spectra and EDS patterns (mol g^{-1} of tungstate or molybdate species).

Sample	LDH	MoO_4^{2-}/WO_4^{2-}		$Mo_7O_{24}^{6-}/W_7O_{24}^{6-}$		Loading by EDS
	λmax (nm)	λmax (nm)	Area (%)	λmax (nm)	Area (%)	
MA-W	189	227	82	271	18	$1.10x10^{-3}$
MA-Mo	206	239	79	305	21	$9.65x10^{-4}$
ZA-W	188	228	69	266	31	$9.45x10^{-4}$
ZA-Mo	205	239	82	308	18	$1.13x10^{-3}$

Three main bands were identified for all solids (Fig. 5). The bands at lower wavelength can be attributed to the LDH (MA or ZA) absorption from blank experiments. The two bands at 227 - 239 nm and 266 – 308 nm are associated, respectively, with MO_4^{2-} and $M_7O_{24}^{6-}$ species according to the literature [69,98]. These absorption bands correspond to O ligand to 4d or 5d orbitals of, respectively, Mo^{6+} and W^{6+} cations. From deconvolution, it can be inferred there was a greater amount of tungstate (82% and 69%) and molybdate anions (79% and 82%) in comparison to heptametallate (18 – 31%).

This result corroborates the result obtained by Raman vibrational spectroscopy for MA-W and MA-Mo, where the presence of $M_7O_{24}^{6-}$ species was associated to the shoulders at 966 and 944 cm^{-1} (Fig. 4-F). Unexpectedly, $W_7O_{24}^{6-}$ and $Mo_7O_{24}^{6-}$ loaded on ZA were not revealed by Raman spectroscopy (Fig. 4).

In view of the results obtained by the characterization techniques, it is possible to infer that different anionic species indeed were immobilized in the synthesized solids, namely molybdate and heptamolybdate or tungstate and heptatungstate. In addition, it appears there were different proportions of these anionic species in the corresponding solids.

Cyclohexane oxidation

The LDH-molybdate and LDH-tungstate catalytic activity was evaluated for the oxidation reaction of the cyclohexane to cyclohexanone and cyclohexanol (K+A mixture), as the main products, using hydrogen peroxide as oxidant agent in acetonitrile as solvent, according to Fig. 6.

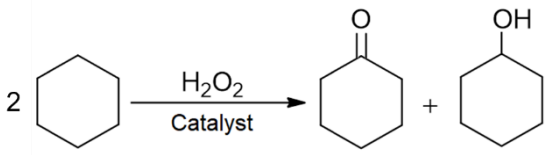

Figure 6. Schematic representation of the catalytic cyclohexane oxidation by hydrogen peroxide, producing the main K+A mixture products (ketone+alcohol).

A reasonably low temperature of 40 °C and excess of solvent acetonitrile (dilute medium) was used to avoid the decomposition of hydrogen peroxide. Nevertheless, it was observed in some cases (discussed later) [69,98]. The catalytic results are presented in Table 3. The control reactions, performed under conditions free of a molybdate and tungstate catalysts, involving only reagents or

reagents with LDH-Cl, showed a very low conversion percentage of cyclohexane either into cyclohexanone ketone (K) or cyclohexanol alcohol (A) (below 0.20% of ketone+alcohol yield).

From Table 3, the conversion of cyclohexane to both ketone (K) and alcohol (A) products, in general increased when using tungstate and molybdate containing LDH in comparison with the control reactions (Table SI-1), suggesting that the W and Mo species have a catalytic contribution to the activation of the oxidizing agent. The conversion results also showed that the catalytic reaction efficiency is dependent on the composition of both the LDH layers (Zn^{2+} or Mg^{2+}) and the oxometallate anions (W or Mo). Despite these reactions, all the catalysts showed selectivity to the ketone products, in general around 60% or higher, consequently better than results presented for other catalysts based on W or Mo (Table SI-2). The best conversion values were observed for ZA-W, the solid combining LDH layers with Zn^{2+} and immobilized tungstate species (W). Comparison of catalyst efficiency showed that, for the same catalytic reaction conditions (3 h reaction time and same catalyst amount), the order of conversion yield (%) followed the decreasing series: ZA-W > MA-W > MA-Mo ≈ ZA-Mo (entries 1-4, Table 3).

ZA-W showed a total conversion percentage yield from cyclohexane to ketone and alcohol products of about 31 times more than ZA-Mo (Table 3, entry 4 - 1.06% in comparison with entry 3 - 0.040%). In fact, some experimental observations during the catalytic reactions shed light on the different catalytic results observed for these two solids.

We observed that at the exact moment of adding the 35% H_2O_2 solution in the reaction medium using the catalyst ZA-Mo, the solid color changed from white to dark red-orange with the concomitant beginning of intense O_2 evolution in the reaction medium. After reaction for 1.5 hours, the O_2 bubbling ceased, and the white color of the catalytic solid returned. The similar solid color change was also expected for the solid containing tungstate species (ZA-W), but it was not perceptible, probably due to the lower concentration of the anionic W species in this ZA (or MA) support (loading), as presented in Table 2. However, unlike the ZA-Mo solid, the ZA-W solid showed no apparent oxygen evolution when mixed with H_2O_2.

469

470 **Table 3.** Conversion of cyclohexane to cyclohexanol alcohol (A) and cyclohexanone ketone (K) by H_2O_2 in the catalytic oxidation reaction[1].

Entry	Cyclohexane (mmol)	H_2O_2 (mmol)	Catalyst (mass/mg)	Reaction time (h)	Yield conversion (%)		Total yield% (%K+%A)[2]	Selectivity of Ketone (%)[3]	Loading (mol g^{-1})	Species estimated by Raman and UV-Vis analyses	MO_4^{2-} (Mol)[4]	$M_7O_{24}^{6-}$ (Mol)[4]
					Ketone (K)	Alcohol (A)						
1	1.0	5.0	MA-Mo (50)	3	0.037	0.025	0.062	60	$9.65x10^{-4}$	MoO_4^{2-} (79%) $Mo_7O_{24}^{6-}$ (21%)	$7.6x10^{-4}$	$2.9x10^{-5}$
2	1.0	5.0	MA-W (50)	3	0.14	0.13	0.27	48	$1.10x10^{-3}$	WO_4^{2-} (82%) $W_7O_{24}^{6-}$ (18%)	$9.0x10^{-4}$	$2.8x10^{-5}$
3	1.0	5.0	ZA-Mo (50)	3	0.024	0.016	0.040	60	$1.13x10^{-3}$	MoO_4^{2-} (82%) $Mo_7O_{24}^{6-}$ (18%)	$9.3x10^{-4}$	$2.9x10^{-5}$
4	1.0	5.0	ZA-W (50)	3	0.67	0.41	1.07	63	$9.45x10^{-4}$	WO_4^{2-} (69%) $W_7O_{24}^{6-}$ (31%)	$6.6x10^{-4}$	$4.1x10^{-5}$
5	1.0	5.0	ZA-W (50)	6	1.75	0.89	2.64	66	$9.45x10^{-4}$	WO_4^{2-} (69%) $W_7O_{24}^{6-}$ (31%)	$6.5x10^{-4}$	$4.2x10^{-5}$
6	1.0	5.0	ZA-W (50)	8	1.83	1.35	3.18	57	$9.45x10^{-4}$	WO_4^{2-} (69%) $W_7O_{24}^{6-}$ (31%)	$6.5x10^{-4}$	$4.2x10^{-5}$
7	1.0	5.0	ZA-W (50)	16	1.97	0.99	2.95	66	$9.45x10^{-4}$	WO_4^{2-} (69%) $W_7O_{24}^{6-}$ (31%)	$6.5x10^{-4}$	$4.2x10^{-5}$
8	0.3	1.0	ZA-W (15)	16	2.44	1.5	3.94	62	$9.45x10^{-4}$	WO_4^{2-} (69%) $W_7O_{24}^{6-}$ (31%)	$6.5x10^{-4}$	$4.2x10^{-5}$
9	0.3	1.0	ZA-W (15)	23	2.32	1.5	3.86	60	$9.45x10^{-4}$	WO_4^{2-} (69%) $W_7O_{24}^{6-}$ (31%)	$6.5x10^{-4}$	$4.2x10^{-5}$
10	1.0	5.0	ZA-W (50)[5]						$9.45x10^{-4}$			
			1 reuse	3	0.52	0.31	0.83	62				
11	1.0	5.0	2 reuse	3	0.43	0.37	0.80	62				
12	1.0	5.0	3 reuse	3	0.43	0.36	0.79	54				
13	1.0	5.0	4 reuse	3	0.41	0.34	0.75	55				

471 [1] General catalytic oxidation reaction conditions: dilute hydrogen peroxide (aqueous solution, 35%), at 40 °C, in the presence of acetonitrile as the solvent, with H_2O_2/substrate molar ratio =
472 5:1. Conversion percentage values based on the initial cyclohexane quantity. [2] Total yield of cyclohexane conversion to K+A = [mols of cyclohexane reacted]/[initial mols of cyclohexane
473 used]x 100 and [3] Ketone product selectivity: [total mol of ketone formed/total mol of cyclohexane converted] x100 [99]. The % conversion values were calculated in at least twice. The error
474 of the results was in the range of 3 to 10%. [4]The mol quantity of all species was calculated based on the loading values (Table 2) and the deconvolution percentage data (Fig. 5). [5]The reuse
475 experiments were performed in reaction conditions similar to those used for the reaction entry 4.

476

Monitoring of H_2O_2 by UV-Vis spectroscopy (Fig. SI-2) allowed comparing the reactivity of ZA-W and ZA-Mo catalysts. Fig. SI-2A shows the electronic spectrum of H_2O_2 (5 mmol) in 3 mL of acetonitrile at a similar concentration (35%) used in the catalytic reaction. The broad band located in the region from 190 nm to 340 nm (maximum at 250 nm) was attributed to the n → σ* electronic transition of the H_2O_2 molecules. The electronic spectra (Fig. SI-2B) of the supernatant of catalytic reaction using ZA-W catalyst were recorded at different reaction times. We observed that H_2O_2 was still available in the reaction medium (band with stronger intensity) even after 3 hours of reaction time, suggesting that even after this time, sufficient H_2O_2 was still present to promote the conversion of cyclohexane to its oxidation products. However, when using ZA-Mo as catalyst, H_2O_2 was fully consumed after 1.5 hours (Fig. SI-2C) and the cyclohexane conversion stopped. H_2O_2 was probably disproportionate in the medium, explaining the intense evolution of oxygen observed in the catalytic reactions promoted by the solid ZA-Mo, unlike the solid ZA-W.

In addition to the intense evolution of oxygen, we also observed an intense dark orange color in the solid ZA-Mo, as previously mentioned. This finding suggests that the color change observed in this ZA-Mo solid may have been directly related to the presence of H_2O_2 in the medium and to the interaction between the oxidant H_2O_2 and the anionic Mo species immobilized in LDH.

To better identify the molybdenum and tungsten species resulting from the presence of H_2O_2 in the medium, UV-Vis spectra of Na_2MoO_4 or Na_2WO_4 aqueous solutions (0.1 mol L^{-1}) were recorded at increasing additions of H_2O_2 amounts. The pH of these solutions was previously adjusted to 8.0 using a 0.1 mol L^{-1} NaOH solution (Figure 7).

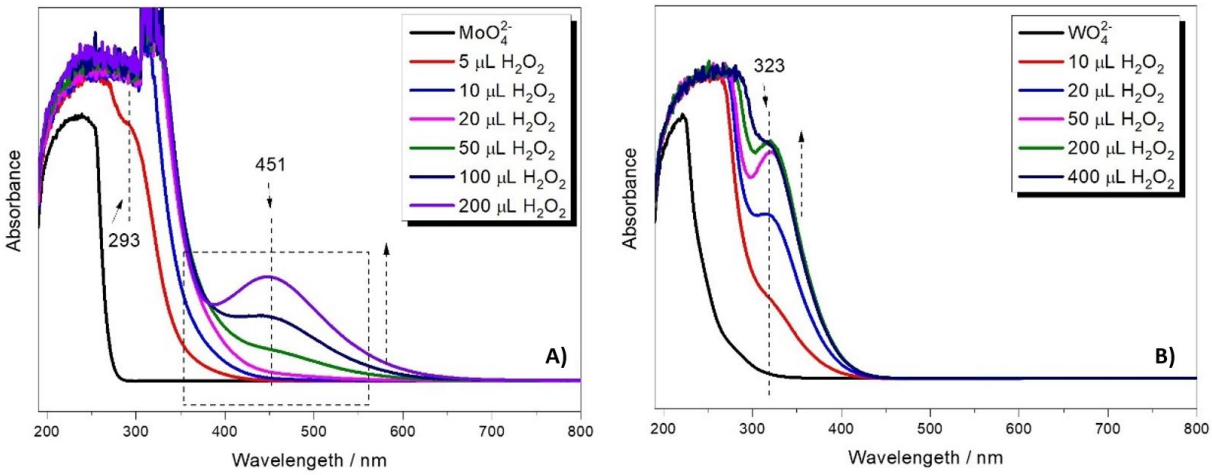

Figure 7. UV-Vis spectra of aqueous solutions of A) Na_2MoO_4 and B) Na_2WO_4 with progressive addition of 35% H_2O_2 solution.

For the aqueous solution of Na_2MoO_4 (Fig. 7B), we observed that before the addition of H_2O_2 the solution was colorless. As the amount of H_2O_2 increased, along with the H_2O_2 adsorption band (250 nm), a new band appeared in the region of 293 nm, whose intensity increased with rising amount of H_2O_2. According to Van Laar et al. [100] and Nardello et al. [71], as the H_2O_2/Mo^{6+} ratio increases, different oxoperoxo-molybdenum species are formed, and the appearance of a band in the region of 293 nm can be attributed to the formation of a di-peroxomolybdate species ($MoO_2(O_2)_2^{2-}$), with a slightly yellowish color (Scheme 1, species 2). After successive addition of H_2O_2, this species was converted into tetra-peroxomolybdate ($Mo(O_2)_4^{2-}$), with red-brown color, and a new band in the region of 450 nm was observed (Scheme 1, species 4) [71,101]. Van Laar [100] also observed that the simultaneous presence of the di- and tetra-peroxomolybdate species in solution indicated that the tri-peroxomolybdate species may also be present as an intermediate species, as indicated by a shoulder in the region of 330 nm (Scheme 1 species 3). This band at 330 nm contributes to the total broad absorption band (Fig. 7A). According to these authors [100,102], when the Mo^{6+} ions interact with H_2O_2, the formed species is responsible for catalyzing the H_2O_2 disproportionation and the different peroxo-species formed are intermediate species in this process, explaining the intense oxygen evolution observed. Interestingly, all peroxomolybdate species displayed the same negative charge (2-). Consequently, conversion of molybdate loaded on the LDH surface into peroxomolybdate did not affect the overall neutrality of the LDH structure, which remained stable under the catalytic reaction conditions.

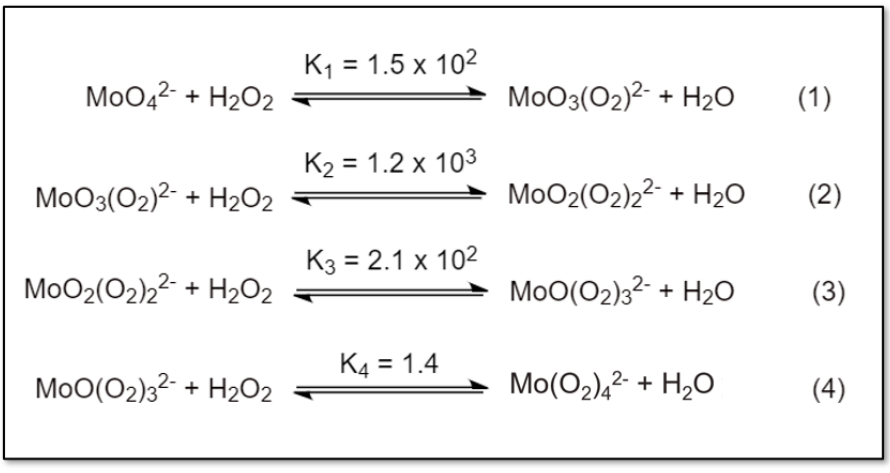

Scheme 1. Representative speciation scheme of peroxomolybdate with increasing H_2O_2/Mo molar ratio [101].

The electronic spectrum observed (Fig.7B) for the Na_2WO_4 solution had a band in the region of 250 nm, and after the successive addition of hydrogen peroxide solution, a shoulder around 323

nm was observed, whose intensity increased with rising amount of H_2O_2. There was no evidence of the formation of any other band, as was observed in the case of the Na_2MoO_4 solution.

Sels et al. [103] observed that the interaction of H_2O_2 with tungstate ions led to the direct formation of tetra-peroxotungstate as a single species, identified by an absorption band around 330 nm. Like the peroxomolybdate, this species is also responsible for catalyzing the disproportionation of H_2O_2, but with slower H_2O_2 disproportionation kinetics. Indeed, as already discussed for Fig. Si-2, H_2O_2 was still available after 3 hours of reaction catalyzed by ZA-W, increasing the efficiency of cyclohexane oxidation.

Therefore, these results confirm that in the presence of H_2O_2, molybdate and tungstate ions led to the formation of peroxo-species, which were responsible for catalyzing the disproportionation reaction of H_2O_2 from the reaction medium, with disproportionate kinetics depending on the nature of the metal ions (W^{6+} or Mo^{6+}).

To gain insight about the oxidation mechanism, the intermediate molybdate (ZA-Mo) and tungstate (ZA-W) catalytic species formation were characterized by *in situ* UV-Vis analysis in the presence of H_2O_2 (35%) during a period of 6 hours for ZA-Mo and 6.1 hours for ZA-W. (Fig. 8).

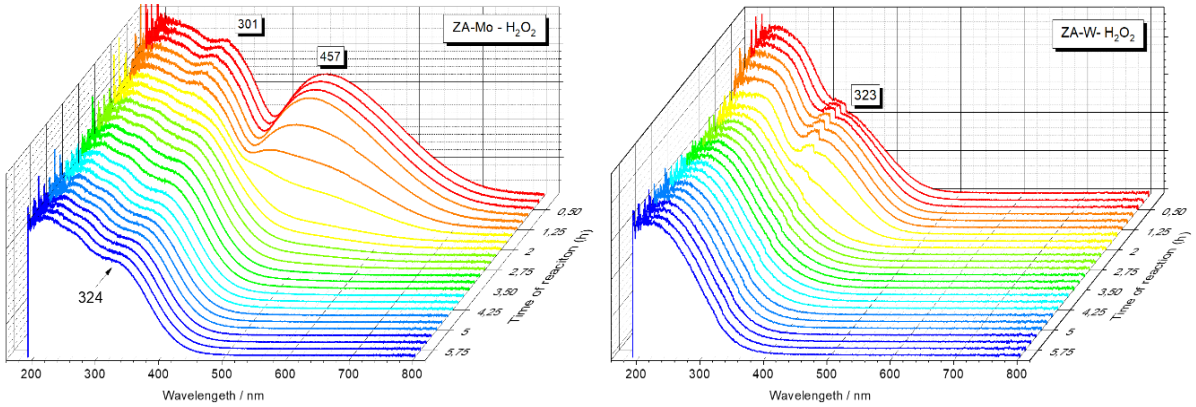

Figure 8. UV-Vis spectra recorded of the supernatant of the catalytic oxidation reaction of cyclohexane with hydrogen peroxide catalyzed by ZA-Mo and ZA-W at different times (Z) using the same reaction conditions described in Table 3.

For the reaction catalyzed by ZA-Mo, peroxomolybdate species appeared at the beginning of the reaction, when H_2O_2 was added. The dispersion immediately became orange. The UV-Vis spectra showed two absorption bands, at 301 nm and 457 nm, indicating the simultaneous formation of diperoxo-molybdate ($MoO_2(O_2)_2^{2-}$) (band at 301 nm) and tetra-peroxomolybdate ($Mo(O_2)_4^{2-}$) (band at

457 nm), similar to that observed for sodium molybdate solutions mixed with H_2O_2 (Fig. 7B). The band at 457 nm disappeared after 2 h and a new band at 324 nm (as a shoulder) was observed and remained for another 4 hours of monitoring (6 hours all told), suggesting the formation of the tri-peroxomolybdate species resulting from the decomposition of tetra-peroxomolybdate species. In fact, because this shoulder at 324 nm was part of a larger and more extended band, probably there was a mixture of species such as molybdates and other peroxomolybdates.

For ZA-W (Fig. 8), only the presence of a large shoulder at 323 nm was observed at the initial moments of the reaction, which can be attributed to the formation of mixtures of species including di- and tetra-peroxotungstate anions. After about 2 h of reaction time, this shoulder disappeared, but the spectral profile remained unchanged up to 6 h, suggesting the presence of a mixture of species, including the tungstate anion WO_4^{2-} initially present in the solid.

Based on these *in situ* data, we can suggest that the presence of H_2O_2 caused the formation of multiple peroxo species, including di-, tri-, and tetra-peroxomolybdate or peroxotungstate catalytic species, attached at the LDH layers' surface. Many studies have reported that the di-peroxo species ($MoO_2(O_2)_2^{2-}$) is the most active species in catalytic reactions combining hydrogen peroxide and either molybdate or tungstate compounds, in solution or immobilized on different supports. Di-peroxometalate species (Mo or W) obtained by the reaction of hydrogen peroxide and solids resulting in the immobilization of MoO_4^{2-} or WO_4^{2-} species on LDHs was reported by Maciuca et al. [69,98] to be an intermediate catalytic species involved in the oxidation reaction of tetrahydrothiophene to sulfolane. Vafaeezadeh et al. also reported that a diperoxo-molybdate species was observed as an intermediate catalytic species involved in the cyclohexene oxidation reaction when a tungstate species immobilized on functionalized silica was used as solid catalyst [50].

The tungstate and molybdate immobilization on the hydroxylated LDH layers' surface did not appear to present a limitation for the formation of intermediate active species and the catalytic oxidation. In particular, the adsorbed molybdate (ZA-Mo) caused greater disproportionation of H_2O_2 and evolution of O_2, which contributed to an unproductive decomposition of H_2O_2 [67], hence leading to less conversion of the cyclohexane into cyclohexanone and cyclohexanol products compared to ZA-W.

Table 3 also shows that for the same W or Mo catalytic species, better conversion yields were observed for the ZnAl LDH immobilization matrix (Table 3, entry 3 versus 4) than for the MgAl support (entry 1 versus 2). A possible explanation is the difference of basicity of the LDH structure, with the MgAl LDH being more basic than the ZnAl LDH due to the difference of electronegativity between Mg and Zn, as shown by catalytic evaluation using aldol condensation [104–107]. The basicity of the support could then affect the speciation of the oxometallate species [68]. It has been widely reported that the peroxo catalytic active species formed by the reaction of WO_4^{2-} (or MoO_4^{2})

and hydrogen peroxide in catalytic oxidation reactions is strongly dependent on the acidity of the reaction medium [6,50,67,68], as shown by Scheme 2.

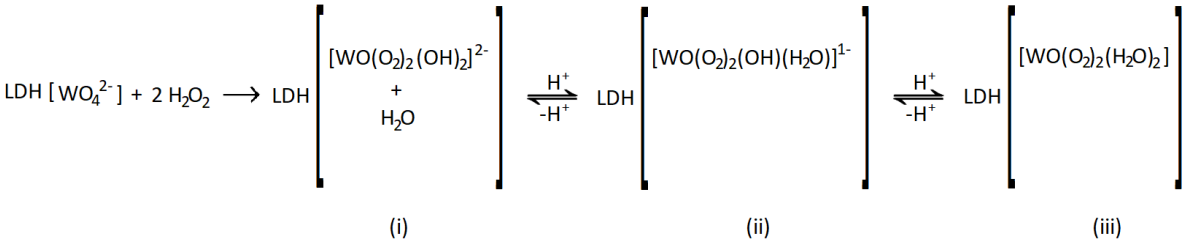

Scheme 2. Schematic representation of the plausible di-peroxocatalytic species obtained by the reaction of tungstate species immobilized on LDH solid with magnesium/aluminum (MA) or zinc/aluminum (ZA) composition [67].

It has been reported that the species obtained (i) by the reaction of tungstate and 2 mol of hydrogen peroxide (Scheme 2) is dependent on the acidity of the reaction medium and can be in equilibrium with both species (ii) and (iii). Species (ii) and (iii) are reported to be more active in the catalytic oxidation reaction [50,67]. Noyori et al. [67] also reported that species (ii) is predominant, mainly in the pH range of 0.4 to 3.0.

The remarkable difference in the catalytic results observed for the solid ZA-W (Table 3, entry 4) compared to solid MA-W (Table 3, entry 2), of about 4.0 times the total yield (%) of ketone + alcohol products, with more pronounced selectivity to ketone for the reaction catalyzed by ZA-W (63% selectivity to ketone, entry 4 compared to 48%, entry 2), suggested that the acidity of the solid support with zinc LDH can favor more active species $[WO(O_2)_2(OH)(H_2O)]^{-1}$ (Scheme 2, ii). A qualitative evaluation of the pH of ZA-W and MA-W dispersions in acetonitrile solvent showed that the pH values were more acid for the ZA-W suspension than for the MA-W suspension, suggesting that pH could be the key parameter affecting the observed catalytic results.

Changes in the pH of the reaction medium can also explain the differences in the observed catalytic results between reactions 7 and 8 (Table 3), where a 1.33-fold increase in the total conversion yield (K+A) (with similar selectivity for the ketone product) from entry 7 to 8 was observed. Indeed, the decrease in cyclohexane/ H_2O_2 molar ratio from 1:5 (entry 7) to 0.3:1 (entry 8) and in catalyst mass from 50 mg (entry 7) to 15 mg (entry 8) led to a decrease of pH value to 8.0 (entry 8). This resulted in a more favorable pH condition for the stabilization of catalytically active species $[WO(O_2)_2(OH)(H_2O)]^{-1}$ (Scheme 2, ii) and $[WO(O_2)_2 (H_2O)_2]$ (Scheme 2, iii).

Vafaeezadeh et al. [50] observed that when the monoprotonated peroxotungstate species (ii) (Scheme 2) decreased, there was a reduction in the conversion of cyclohexene to oxidation products,

and this fact was attributed to the increase of the reaction from 0.89 to 1.08, caused by increasing the molar ratio of cyclohexene/H_2O_2 from 1:4 to 1:6. Unfortunately, it is difficult to determine the reaction pH in organic media under the experimental conditions used, and the apparent pH values of the reaction solutions 7 and 8 were not determined.

In addition, the effect of reaction time on the cyclohexane conversion yield in the reactions catalysed by ZA-W and the selectivity for the related products were studied. The effect of reaction time is reported in entries 4 to 9 (Table 3). We clearly observed that increasing the reaction time (from 3 to 23 h), regardless of the mass of catalyst used or molar ratio of cyclohexane/H_2O_2, caused the total yield of cyclohexane conversion into (ketone+alcohol) to increase. For the first 6 hours, the conversion yield (similar conditions, entries 4 to 7) increased nearly linearly (+ 0.41% h^{-1}) before stabilizing at a value of about 3.8-3.9%. This general trend was confirmed under different cyclohexane/H_2O_2 and catalyst mass conditions (entries 8 and 9). Moreover, the selectivity to the ketone product remained almost constant between 60 and 66%, independent of the various reaction conditions (reaction time, reagent composition, catalyst mass). These results suggest stability of the product over long reaction times, as reported by Jing Dai et al. [6]. Rezaei at al. [99] observed an optimum conversion time of 4 h for the oxidation reaction of cyclohexane by hydrogen peroxide to ketone and alcohol (conversion value of 6.59%) catalyzed by vanadyl pyrophosphate supported on mesoporous silica. When the reaction time was increased to 16 h, decreases of conversion yield and byproduct formation, including 1,3-cyclohexanediol, 1,4-cyclohexanedione and 4-hydroxylcyclohexanone, were observed.

It is well known that metalloporphyrins (MP) are efficient catalysts for cyclohexane oxidation under mild experimental condition (room temperature and 30 minutes reaction time). Depending on the structure of the porphyrin ligand and the metal ions of the MP complex, using different oxidant species (H_2O_2, peracids, iodosylbenzene, O_2, etc.), promising yields of alcohol (majority product) and ketone have been consistently observed [13–15,108–111].

Nan et al. reported the catalytic results of cyclohexane and other alkanes and alkenes oxidized by 30% H_2O_2 using iron(III) porphyrin [Fe(TPFPP)X] (where X^{1-} = axial anionic ligand of the Fe^{3+}-complex), finding it to be a very efficient metalloporphyrin catalyst for epoxidation and hydroxylation of different organic substrates in a biomimetic model of cytochrome P-450 [112]. Depending on the value of X^{1-}, they observed very good results of alcohol and ketone. For example, the best results were alcohol yield of 30% and ketone yield of 1% (using Fe(TPFPP)NO_3 as catalyst ($1x10^{-3}$ mmol), H_2O_2 (0.02 mmol/0.5 mL CH_3CN), cyclohexane (1 mmol) in a solvent mixture of CH_3CN/CH_2Cl_2 (3:1), for 1 h of reaction under stirring). However, when the yields reported based on the amount of H_2O_2 used were converted into percentage of conversion of the substrate to both products (as used in this work to describe the catalytic results of the solids ZA-W and the others – see

footnote of Table 3) the catalytic results were 0.060% conversion to alcohol and 0.002% to ketone, with total conversion yield of 0.062%, similar to the total yield observed for the catalyst MA-Mo (Table 3, entry 1). This was far from the best result of the catalyst studied here, ZA-W, which in non-optimized condition (Table 3, entry 4) presented a total yield 1.07%, about 17 times higher than the result when using iron porphyrin.

Despite the pronounced selectivity of the iron porphyrin to the alcohol product and the ZA-W to the ketone product, the results presented in Table 3 demonstrated that the solids studied in this work are comparable to the metalloporphyrin catalyst for the cyclohexane oxidation under the investigated experimental conditions using H_2O_2 as oxidant.

Finally, catalyst recycling experiments were carried out by reusing the ZA-W, 4 times. The recycling results are shown in Table 3, entries 10 to 13 and Figure 9. The recycling conditions were the same as those in the first use of the catalyst (Table 3, entry 4). The conversion of cyclohexane to ketone+alcohol products and selectivity to ketone did present a decrease of 22% in yield between the first and second reactions, which could be attributed to the loss of outermost tungstate anions decorating the solid. However, from the third to the fifth reaction, there's less than 10% of decrease in yield, suggesting that what remains of the catalytic species is quite stable in the LDH and the solid is suitable for heterogeneous processes.

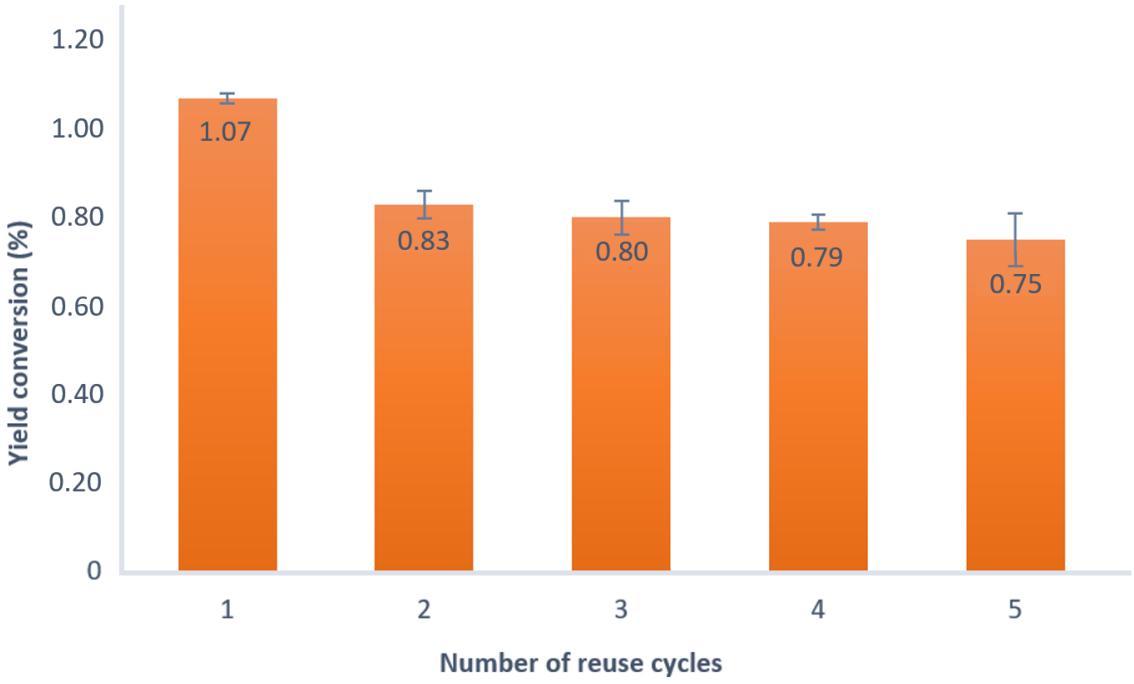

Figure 9. Cyclohexane yield conversion versus number of reuses.

Conclusion

Researchers are seeking to develop new materials able to catalyze organic synthesis according to the tenets of green chemistry, i.e., economy of atoms, reaction stages and energy; and less harm to the environment through sustainable and recyclable processes. Among the targeted reactions, oxidation of alkane is still a hot topic that is widely investigated, particularly the selective production of ketones and alcohols from alkanes using H_2O_2, a cheap and environmentally friendly reagent. Mono-molybdate and mono-tungstate are known for their catalytic reactivity towards the oxidation of alkanes by H_2O_2 in homogeneous media.

This study highlights the potential of layered double hydroxides as supports for mono-molybdate and mono-tungstate for the catalytic oxidation of cyclohexane to cyclohexanone and cyclohexanol. Due to their unique anion exchange properties, we were able to immobilize high amounts of mono-molybdate (MoO_4^{2-}) and mono-tungstate (WO_4^{2-}) on the LDH matrices ZnAl (resp. $1.13x10^{-3}$ and $9.45x10^{-4}$ mol g^{-1}) and MgAl HDL (resp. $9.65x10^{-4}$ and $1.10x10^{-3}$ mol g^{-1}). During the intercalation step, the LDH structure was preserved, with the oxometallates being mainly distributed on the platelet surfaces.

The prepared HDL/oxometallate showed outstanding catalytic activity towards the oxidation of cyclohexane by H_2O_2, leading to the conversion to cyclohexanone and cyclohexanol. The maximum conversion yield obtained reached 3.94% (ZA-W). Improvement was possible by increasing the catalytic conditions (quantity of catalysts, temperature). The selectivity towards ketone reached a value of 66% (ZA-W). Probably due to a lower basicity of the ZA LDH and a moderate reactivity of WO_4^{2-} compared to the MoO_4^{2-} species, the ZA-W supported catalyst was the most efficient catalyst for the conversion of cyclohexane into related ketone and alcohol.

Peroxomolybdate and peroxtungstate intermediates were identified by UV-Vis spectroscopy, demonstrating that their immobilization on LDH supports favored the formation of these reactive catalytic species. Nevertheless, the high reactivity of MoO_4^{2-} caused the disproportionation of H_2O_2 and the abundant evolution of molecular oxygen, which inactivated the oxidant and limited the oxidation of cyclohexane. In the case of the ZA-W phases, the most stable diperoxotungstate species was an efficient catalyst. In addition, the recycling of the ZA-W catalyst over 5 cycles showed maintenance of the conversion rate up to 75%.

In conclusion, the solid catalyst developed in this work based on LDH support provides structural and thermal stability and they are recyclable. The solid catalysts are also very versatile, as the tungstate and molybdate ions are known to be applied in a range of different reactions. Last but not the least, the material developed in this work achieved good yield in mild reaction conditions, not needing excessive heating or elevated pressures.

Acknowledgements

We are grateful to Coordenação de Aperfeiçoamento de Pessoal de Nível Superior (CAPES – Finance code 001 and CAPES-PrInt/PROCESSO 88881.311981/2018-01), Conselho Nacional de Desenvolvimento Científico e Tecnológico (CNPq: SN projects 301876/2019-3 and 405217/2018-8; FW Project 300988/2019-2), Fundação Araucária, and Centro de Microscopia da UFPR (CME/UFPR).

References

[1] J.M. Thomas, R. Raja, G. Sankar, R.G. Bell, Molecular-sieve catalysts for the selective oxidation of linear alkanes by molecular oxygen, Nature. 398 (1999) 227–230. https://doi.org/10.1038/18417.

[2] M. Bordeaux, A. Galarneau, J. Drone, Catalytic, Mild, and Selective Oxyfunctionalization of Linear Alkanes: Current Challenges, Angew. Chemie Int. Ed. 51 (2012) 10712–10723. https://doi.org/10.1002/anie.201203280.

[3] K.C. Hwang, A. Sagadevan, One-pot room-temperature conversion of cyclohexane to adipic acid by ozone and UV light, Science. 346 (2014) 1495–1498. https://doi.org/10.1126/science.1259684.

[4] Merchant Research and Consulting, Adipic Acid (ADPA), 2018 World Market Outlook and Forecast up to 2027, Birmingham, UK, 2018.

[5] J. Luo, Y. Huang, B. Ding, P. Wang, X. Geng, J. Zhang, Y. Wei, Single-Atom Mn Active Site in a Triol-Stabilized β-Anderson Manganohexamolybdate for Enhanced Catalytic Activity towards Adipic Acid Production, Catalysts. 8 (2018) 121. https://doi.org/10.3390/catal8030121.

[6] J. Dai, W. Zhong, W. Yi, M. Liu, L. Mao, Q. Xu, D. Yin, Bifunctional H2WO4/TS-1 catalysts for direct conversion of cyclohexane to adipic acid: Active sites and reaction steps, Appl. Catal. B Environ. 192 (2016) 325–341. https://doi.org/10.1016/j.apcatb.2016.04.005.

[7] ~~J. Zhang, J. Liu, X. Wang, J. Mai, W. Zhao, Z. Ding, Y. Fang, Construction of Z-scheme tungsten trioxide-nanosheets-nitrogen-doped carbon dots composites for the enhanced photothermal synergistic catalytic oxidation of cyclohexane, Appl. Catal. B Environ. 259 (2019) 118063. https://doi.org/10.1016/j.apcatb.2019.118063.~~

[8] O. Perraud, A.B. Sorokin, J.-P. Dutasta, A. Martinez, Oxidation of cycloalkanes by H2O2 using a copper–hemicryptophane complex as a catalyst, Chem. Commun. 49 (2013) 1288. https://doi.org/10.1039/c2cc37829a.

[9] G. Olivo, O. Cussó, M. Borrell, M. Costas, Oxidation of alkane and alkene moieties with biologically inspired nonheme iron catalysts and hydrogen peroxide: from free radicals to stereoselective transformations, JBIC J. Biol. Inorg. Chem. 22 (2017) 425–452. https://doi.org/10.1007/s00775-016-1434-z.

[10] ~~M. V. Kirillova, T.A. Fernandes, V. André, A.M. Kirillov, Mild C–H functionalization of alkanes catalyzed by bioinspired copper(II) cores, Org. Biomol. Chem. 17 (2019) 7706–7714. https://doi.org/10.1039/C9OB01442J.~~

[11] F.A. Chavez, J.M. Rowland, M.M. Olmstead, P.K. Mascharak, Syntheses, Structures, and Reactivities of Cobalt(III)−Alkylperoxo Complexes and Their Role in Stoichiometric and Catalytic Oxidation of Hydrocarbons, J. Am. Chem. Soc. 120 (1998) 9015–9027. https://doi.org/10.1021/ja9814873.

[12] L. Ma, Y. Pan, W.-L. Man, H.-K. Kwong, W.W.Y. Lam, G. Chen, K.-C. Lau, T.-C. Lau, Highly Efficient Alkane Oxidation Catalyzed by [Mn V (N)(CN) 4] 2– . Evidence for [Mn VII (N)(O)(CN) 4] 2– as an Active Intermediate, J. Am. Chem. Soc. 136 (2014) 7680–7687. https://doi.org/10.1021/ja5019546.

[13] S. Nakagaki, K.A.D.F. Castro, G.M. Ucoski, M. Halma, V. Prévot, C. Forano, F. Wypych, Anionic Iron(III) Porphyrin Immobilized on/into Exfoliated Macroporous Layered Double Hydroxides as Catalyst for Oxidation Reactions, J. Braz. Chem. Soc. 25 (2014) 2329–2338. https://doi.org/10.5935/0103-5053.20140241.

[14] J.T. Groves, T.E. Nemo, R.S. Myers, Hydroxylation and epoxidation catalyzed by iron-porphine complexes. Oxygen transfer from iodosylbenzene, J. Am. Chem. Soc. 101 (1979) 1032–1033. https://doi.org/10.1021/ja00498a040.

[15] K.C.M. Westrup, R.M. Silva Jr., K.M. Mantovani, L. Bach, J.F. Stival, P.G.P. Zamora, F. Wypych, G.S. Machado, S. Nakagaki, Light-assisted cyclohexane oxidation catalysis by a manganese(III) porphyrin immobilized onto zinc hydroxide salt and zinc oxide obtained by zinc hydroxide salt hydrothermal decomposition, Appl. Catal. A Gen. 602 (2020) 117708. https://doi.org/10.1016/j.apcata.2020.117708.

[16] K.M. Mantovani, J.F. Stival, F. Wypych, L. Bach, P.G. Peralta Zamora, M. Luiza Rocco, S. Nakagaki, Unusual catalytic activity after simultaneous immobilization of two metalloporphyrins on hydrozincite/nanocrystalline anatase, J. Catal. 352 (2017) 442–451. https://doi.org/10.1016/j.jcat.2017.06.015.

[17] ~~C.-M. Che, J.-S. Huang, Metalloporphyrin-based oxidation systems: from biomimetic reactions to application in organic synthesis, Chem. Commun. (2009) 3996–4015. https://doi.org/10.1039/b901221d.~~

[18] C.L. Hill, R.D. Gall, The first combinatorially prepared and evaluated inorganic catalysts. Polyoxometalates for the aerobic oxidation of the mustard analog tetrahydrothiophene (THT), J. Mol. Catal. A Chem. 114 (1996) 103–111. https://doi.org/10.1016/S1381-1169(96)00308-1.

[19] I. V. KOZHEVNIKOV, Heteropoly Acids and Related Compounds as Catalysts for Fine Chemical Synthesis, Catal. Rev. 37 (1995) 311–352. https://doi.org/10.1080/01614949508007097.

[20] C.L. Hill, C.M. Prosser-McCartha, Homogeneous catalysis by transition metal oxygen anion clusters, Coord. Chem. Rev. 143 (1995) 407–455. https://doi.org/10.1016/0010-8545(95)01141-B.

[21] B.M. Choudary, N.S. Chowdari, S. Madhi, M.L. Kantam, A Trifunctional Catalyst for One-Pot Synthesis of Chiral Diols via Heck Coupling−N-Oxidation−Asymmetric Dihydroxylation: Application for the Synthesis of Diltiazem and Taxol Side Chain, J. Org. Chem. 68 (2003) 1736–1746. https://doi.org/10.1021/jo026687i.

[22] T. Kwon, G.A. Tsigdinos, T.J. Pinnavaia, Pillaring of layered double hydroxides (LDH's) by polyoxometalate anions, J. Am. Chem. Soc. 110 (1988) 3653–3654. https://doi.org/10.1021/ja00219a048.

[23] M.A. Drezdzon, Synthesis of isopolymetalate-pillared hydrotalcite via organic-anion-pillared precursors, Inorg. Chem. 27 (1988) 4628–4632. https://doi.org/10.1021/ic00298a024.

[24] ~~Mark A. Drezdon, Pillared hydrotalcites, 4774212, 1988. https://patents.justia.com/patent/4774212.~~

[25] K. Chibwe, W. Jones, Synthesis of polyoxometalate pillared layered double hydroxides via calcined precursors, Chem. Mater. 1 (1989) 489–490. https://doi.org/10.1021/cm00005a006.

[26] K. Chibwe, W. Jones, Intercalation of organic and inorganic anions into layered double hydroxides, J. Chem. Soc. Chem. Commun. (1989) 926. https://doi.org/10.1039/c39890000926.

[27] E. Narita, P. Kaviratna, T.J. Pinnavaia, Synthesis of Heteropolyoxometalate Pillared Layered Double Hydroxides via Calcined Zinc-Aluminium Oxide Precursors, Chem. Lett. 20 (1991) 805–808. https://doi.org/10.1246/cl.1991.805.

[28] E.D. Dimotakis, T.J. Pinnavaia, New route to layered double hydroxides intercalated by organic anions: precursors to polyoxometalate-pillared derivatives, Inorg. Chem. 29 (1990) 2393–2394. https://doi.org/10.1021/ic00338a001.

[29] J. Wang, Y. Tian, R.C. Wang, A. Clearfield, Pillaring of layered double hydroxides with polyoxometalates in aqueous solution without use of preswelling agents, Chem. Mater. 4 (1992) 1276–1282. https://doi.org/10.1021/cm00024a030.

[30] E. Narita, P.D. Kaviratna, T.J. Pinnavaia, Direct synthesis of a polyoxometallate-pillared layered double hydroxide by coprecipitation, J. Chem. Soc. Chem. Commun. (1993) 60. https://doi.org/10.1039/c39930000060.

[31] J. Luo, Y. Huang, B. Ding, P. Wang, X. Geng, J. Zhang, Y. Wei, Single-Atom Mn Active Site in a Triol-Stabilized β-Anderson Manganohexamolybdate for Enhanced Catalytic Activity towards Adipic Acid Production, Catalysts. 8 (2018) 121–134. https://doi.org/10.3390/catal8030121.

[32] M. Conte, X. Liu, D.M. Murphy, S.H. Taylor, K. Whiston, G.J. Hutchings, Insights into the Reaction Mechanism of Cyclohexane Oxidation Catalysed by Molybdenum Blue Nanorings, Catal. Letters. 146 (2016) 126–135. https://doi.org/10.1007/s10562-015-1660-y.

[33] J. Alcañiz-Monge, G. Trautwein, A. Garcia-Garcia, Influence of peroxometallic intermediaries present on polyoxometalates nanoparticles surface on the adipic acid synthesis, J. Mol. Catal. A Chem. 394 (2014) 211–216. https://doi.org/10.1016/j.molcata.2014.07.023.

[34] T. Tatsumi, K. Yamamoto, H. Tajima, H. Tominaga, Shape Selective Epoxidation of Alkenes Catalyzed by Polyoxometalate-Intercalated Hydrotalcite, Chem. Lett. 21 (1992) 815–818. https://doi.org/10.1246/cl.1992.815.

[35] T. Tatsumi, K. Yamamoto, H. Tajima, H. Tominaga, New Frontiers in Catalysis, 1st ed., Elselvier, Amsterdam, 1993.

[36] A.A. Gonzalez, K. Zhang, S.P. Nolan, R. Lopez de la Vega, S.L. Mukerjee, C.D. Hoff, G.J. Kubas, Thermodynamic and kinetic studies of the complexes W(CO)3(PCy3)2L (L = H2, N2, NCCH3, pyridine, P(OMe)3, CO), Organometallics. 7 (1988) 2429–2435. https://doi.org/10.1021/om00102a001.

[37] S.-S. Sun, D.T. Tran, O.S. Odongo, A.J. Lees, Photophysical and Photochemical Properties of W(0) and Re(I) Carbonyl Complexes Incorporating Ferrocenyl-Substituted Pyridine Ligands, Inorg. Chem. 41 (2002) 132–135. https://doi.org/10.1021/ic010713y.

[38] A.S. Pronin, Y.M. Gayfulin, T.S. Sukhikh, A.N. Lavrov, V. V. Yanshole, Y. V. Mironov, Heterometallic Re/Mo and Re/W cubane-type cluster complexes, Inorg. Chem. Front. 9 (2022) 186–194. https://doi.org/10.1039/D1QI01230D.

[39] W.-Q. Zhang, A.J. Atkin, I.J.S. Fairlamb, A.C. Whitwood, J.M. Lynam, Synthesis and Reactivity of

Molybdenum Complexes Containing Functionalized Alkynyl Ligands: A Photochemically Activated CO-Releasing Molecule (PhotoCO-RM), Organometallics. 30 (2011) 4643–4654. https://doi.org/10.1021/om200495h.

[40] Y. Tanabe, Y. Sekiguchi, H. Tanaka, A. Konomi, K. Yoshizawa, S. Kuriyama, Y. Nishibayashi, Preparation and reactivity of molybdenum complexes bearing pyrrole-based PNP-type pincer ligand, Chem. Commun. 56 (2020) 6933–6936. https://doi.org/10.1039/D0CC02852E.

[41] J. Mai, Y. Fang, J. Liu, J. Zhang, X. Cai, Y. Zheng, Simple synthesis of WO3-Au composite and their improved photothermal synergistic catalytic performance for cyclohexane oxidation, Mol. Catal. 473 (2019) 110389–110395. https://doi.org/10.1016/j.mcat.2019.04.018.

[42] Y. Xiao, J. Liu, J. Mai, C. Pan, X. Cai, Y. Fang, High-performance silver nanoparticles coupled with monolayer hydrated tungsten oxide nanosheets: The structural effects in photocatalytic oxidation of cyclohexane, J. Colloid Interface Sci. 516 (2018) 172–181. https://doi.org/10.1016/j.jcis.2018.01.057.

[43] J. Long, H. Liu, S. Wu, S. Liao, Y. Li, Selective Oxidation of Saturated Hydrocarbons Using Au–Pd Alloy Nanoparticles Supported on Metal–Organic Frameworks, ACS Catal. 3 (2013) 647–654. https://doi.org/10.1021/cs300754k.

[44] Y. Shiraishi, Y. Sugano, S. Ichikawa, T. Hirai, Visible light-induced partial oxidation of cyclohexane on WO3 loaded with Ptnanoparticles, Catal. Sci. Technol. 2 (2012) 400–405. https://doi.org/10.1039/C1CY00331C.

[45] S.S. Acharyya, S. Ghosh, R. Bal, Nanoclusters of Cu(II) supported on nanocrystalline W(VI) oxide: a potential catalyst for single-step conversion of cyclohexane to adipic acid, Green Chem. 17 (2015) 3490–3499. https://doi.org/10.1039/C5GC00379B.

[46] K. Sato, M. Aoki, R. Noyori, A “Green” Route to Adipic Acid: Direct Oxidation of Cyclohexenes with 30 Percent Hydrogen Peroxide, Science (80-.). 281 (1998) 1646–1647. https://doi.org/10.1126/science.281.5383.1646.

[47] S. Ghosh, S.S. Acharyya, S. Adak, L.N.S. Konathala, T. Sasaki, R. Bal, Selective oxidation of cyclohexene to adipic acid over silver supported tungsten oxide nanostructured catalysts, Green Chem. 16 (2014) 2826–2834. https://doi.org/10.1039/c4gc00130c.

[48] M. Shang, T. Noël, Q. Wang, Y. Su, K. Miyabayashi, V. Hessel, S. Hasebe, 2- and 3-Stage temperature ramping for the direct synthesis of adipic acid in micro-flow packed-bed reactors, Chem. Eng. J. 260 (2015) 454–462. https://doi.org/10.1016/j.cej.2014.08.061.

[49] Y. Usui, K. Sato, A green method of adipic acid synthesis: organic solvent- and halide-free oxidation of cycloalkanones with 30% hydrogen peroxide, Green Chem. 5 (2003) 373–375. https://doi.org/10.1039/b305847f.

[50] M. Vafaeezadeh, M. Mahmoodi Hashemi, Simple and green oxidation of cyclohexene to adipic acid with an efficient and durable silica-functionalized ammonium tungstate catalyst, Catal. Commun. 43 (2014) 169–172. https://doi.org/10.1016/j.catcom.2013.10.001.

[51] M. Sutradhar, A.P.C. Ribeiro, M.F.C. Guedes da Silva, A.M.F. Palavra, A.J.L. Pombeiro, Application of molybdenum complexes for the oxidation of cyclohexane in acetonitrile, ionic liquid and supercritical CO2 media, a comparative study, Mol. Catal. 482 (2020) 100356–100366. https://doi.org/10.1016/j.mcat.2017.10.026.

[52] R.K. Rana, B. Viswanathan, Mo incorporation in MCM-41 type zeolite, Catal. Letters. 52 (1998) 25–29. https://doi.org/https://doi.org/10.1023/A:1019019403375.

[53] N.J. Campbell, A.C. Dengel, C.J. Edwards, W.P. Griffith, Studies on transition metal peroxo complexes. Part 8. The nature of peroxomolybdates and peroxotungstates in aqueous solution, J. Chem. Soc. Dalt. Trans. (1989) 1203–1208. https://doi.org/10.1039/dt9890001203.

[54] M. Amini, M.M. Haghdoost, M. Bagherzadeh, Oxido-peroxido molybdenum(VI) complexes in catalytic and stoichiometric oxidations, Coord. Chem. Rev. 257 (2013) 1093–1121. https://doi.org/10.1016/j.ccr.2012.11.018.

[55] M.G. Buonomenna, G. Golemme, M.P. De Santo, E. Drioli, Direct Oxidation of Cyclohexene with Inert Polymeric Membrane Reactor, Org. Process Res. Dev. 14 (2010) 252–258. https://doi.org/10.1021/op900022t.

[56] T. Hibino, Acid Treatment of Layered Double Hydroxides Containing Carbonate, Eur. J. Inorg. Chem. 2014 (2014) 5311–5321. https://doi.org/10.1002/ejic.201402372.

[57] N. Iyi, T. Matsumoto, Y. Kaneko, K. Kitamura, Deintercalation of Carbonate Ions from a Hydrotalcite-Like Compound: Enhanced Decarbonation Using Acid−Salt Mixed Solution, Chem. Mater. 16 (2004) 2926–2932. https://doi.org/10.1021/cm049579g.

[58] P. LIU, H. WANG, Z. FENG, P. YING, C. LI, Direct immobilization of self-assembled polyoxometalate catalyst in layered double hydroxide for heterogeneous epoxidation of olefins, J. Catal. 256 (2008) 345–348. https://doi.org/10.1016/j.jcat.2008.03.022.

[59] P. Levecque, H. Poelman, P. Jacobs, D. De Vos, B. Sels, Regio- and stereoselective terpene epoxidation using tungstate-exchanged takovites: a study of phase purity, takovite composition and stable catalytic activity, Phys. Chem. Chem. Phys. 11 (2009) 2964–2975. https://doi.org/10.1039/b820336a.

[60] K. Colombo, S. Maruyama, C. Yamamoto, F. Wypych, Intercalation of Molybdate Ions into Ni/Zn Layered Double Hydroxide Salts: Synthesis, Characterization, and Preliminary Catalytic Activity in Methyl Transesterification of Soybean Oil, J. Braz. Chem. Soc. 28 (2017) 1315–1322. https://doi.org/10.21577/0103-5053.20160298.

[61] B.F. Sels, D.E. De Vos, P.A. Jacobs, Bromide-Assisted Oxidation of Substituted Phenols with Hydrogen Peroxide to the Corresponding p-Quinol and p-Quinol Ethers over WO42- -Exchanged Layered Double Hydroxides, Angew. Chemie Int. Ed. 44 (2005) 310–313. https://doi.org/10.1002/anie.200461555.

[62] U.S. Agarwalla, Mo- and W-containing layered double hydroxides: Mild and selective oxidation of alkenes with H2O2, Indian J. Chem. - Sect. A. 60 (2021) 656–662. http://op.niscair.res.in/index.php/IJCA/article/view/42530.

[63] J. Wahlen, D.E. De Vos, B.F. Sels, V. Nardello, J.-M. Aubry, P.L. Alsters, P.A. Jacobs, Molybdate-exchanged layered double hydroxides for the catalytic disproportionation of hydrogen peroxide into singlet oxygen: Evaluation and improvements of 1O2 generation by combined chemiluminescence and trapping experiments, Appl. Catal. A Gen. 293 (2005) 120–128. https://doi.org/10.1016/j.apcata.2005.07.014.

[64] C. Yuan, H. Liu, X. Gao, Magnetically Recoverable Heterogeneous Catalyst: Tungstate Intercalated Mg–Al-Layered Double Hydroxides-Encapsulated Fe3O4 Nanoparticles for Highly

Efficient Selective Oxidation of Sulfides with H2O2, Catal. Letters. 144 (2014) 16–21. https://doi.org/10.1007/s10562-013-1129-9.

[65] E. V. Korneeva, A.S. Ivanova, V.M. Bondareva, L.M. Plyasova, T.S. Glazneva, Structural, textural, and acid–base properties of layered Mg–Al oxides modified with a tungstate or phosphate and their activity and selectivity in gas-phase glycerol dehydration, Kinet. Catal. 56 (2015) 605–616. https://doi.org/10.1134/S0023158415050109.

[66] S. Zhao, J. Xu, M. Wei, Y.-F. Song, Synergistic catalysis by polyoxometalate-intercalated layered double hydroxides: oximation of aromatic aldehydes with large enhancement of selectivity, Green Chem. 13 (2011) 384. https://doi.org/10.1039/c0gc00664e.

[67] R. Noyori, M. Aoki, K. Sato, Green oxidation with aqueous hydrogen peroxide, Chem. Commun. (2003) 1977–1986. https://doi.org/10.1039/b303160h.

[68] E. Gardner, T.J. Pinnavaia, On the nature of selective olefin oxidation catalysts derived from molybdate- and tungstate-intercalated layered double hydroxides, Appl. Catal. A Gen. 167 (1998) 65–74. https://doi.org/10.1016/S0926-860X(97)00299-8.

[69] A.-L. Maciuca, C.-E. Ciocan, E. Dumitriu, F. Fajula, V. Hulea, V-, Mo- and W-containing layered double hydroxides as effective catalysts for mild oxidation of thioethers and thiophenes with H2O2, Catal. Today. 138 (2008) 33–37. https://doi.org/10.1016/j.cattod.2008.04.031.

[70] G.-J. ten Brink, I.W.C.E. Arends, R.A. Sheldon, Green, Catalytic Oxidation of Alcohols in Water, Science (80-.). 287 (2000) 1636–1639. https://doi.org/10.1126/science.287.5458.1636.

[71] V. Nardello, J. Marko, G. Vermeersch, J.M. Aubry, 90Mo NMR and kinetic studies of peroxomolybdic intermediates involved in the catalytic disproportionation of hydrogen peroxide by molybdate ions, Inorg. Chem. 34 (1995) 4950–4957. https://doi.org/10.1021/ic00124a007.

[72] B.F. Sels, D.E. De Vos, P.J. Grobet, F. Pierard, F. Kirsch-De Mesmaeker, P.A. Jacobs, Molybdate- and Tungstate-Exchanged Layered Double Hydroxides as Catalysts for 1O2 Formation: Characterization of Reactive Oxygen Species and a Critical Evaluation of 1O2 Detection Methods, J. Phys. Chem. B. 103 (1999) 11114–11123. https://doi.org/10.1021/jp992236z.

[73] N. Iyi, H. Yamada, One-step Conversion of CO3 2− LDH (Layered Double Hydroxide) into Anion-exchangeable LDHs Using an Acetate-buffer/Salt Method, Chem. Lett. 39 (2010) 591–593. https://doi.org/10.1246/cl.2010.591.

[74] N. Iyi, H. Yamada, Efficient decarbonation of carbonate-type layered double hydroxide (CO32−LDH) by ammonium salts in alcohol medium, Appl. Clay Sci. 65–66 (2012) 121–127. https://doi.org/10.1016/j.clay.2012.05.001.

[75] S.S.C. Pushparaj, C. Forano, V. Prevot, A.S. Lipton, G.J. Rees, J. V. Hanna, U.G. Nielsen, How the Method of Synthesis Governs the Local and Global Structure of Zinc Aluminum Layered Double Hydroxides, J. Phys. Chem. C. 119 (2015) 27695–27707. https://doi.org/10.1021/acs.jpcc.5b09490.

[76] S. Nakagaki, K. Mantovani, G.S. Machado, K.A.D.F. Castro, F. Wypych, G. Sippel Machado, K. Dias de Freitas Castro, F. Wypych, Recent Advances in Solid Catalysts Obtained by Metalloporphyrins Immobilization on Layered Anionic Exchangers: A Short Review and Some New Catalytic Results, Molecules. 21 (2016) 291.

https://doi.org/10.3390/molecules21030291.

[77] E.S. Zhitova, S. V. Krivovichev, I. Pekov, H.C. Greenwell, Crystal chemistry of natural layered double hydroxides. 5. Single-crystal structure refinement of hydrotalcite, [Mg6Al2(OH)16](CO3)(H2O)4, Mineral. Mag. 83 (2019) 269–280. https://doi.org/10.1180/mgm.2018.145.

[78] N. Iyi, K. Fujii, K. Okamoto, T. Sasaki, Factors influencing the hydration of layered double hydroxides (LDHs) and the appearance of an intermediate second staging phase, Appl. Clay Sci. 35 (2007) 218–227. https://doi.org/10.1016/j.clay.2006.08.011.

[79] L. Claes, R. Matthessen, I. Rombouts, I. Stassen, T. De Baerdemaeker, D. Depla, J.A. Delcour, B. Lagrain, D.E. De Vos, Bio-Based Nitriles from the Heterogeneously Catalyzed Oxidative Decarboxylation of Amino Acids, ChemSusChem. 8 (2015) 345–352. https://doi.org/10.1002/cssc.201402801.

[80] M. Khitous, Z. Salem, D. Halliche, Effect of interlayer anions on chromium removal using Mg–Al layered double hydroxides: Kinetic, equilibrium and thermodynamic studies, Chinese J. Chem. Eng. 24 (2016) 433–445. https://doi.org/10.1016/j.cjche.2015.11.018.

[81] N. Thomas, Synthesis of 3R 1 and 1H Polytypes of Sulfate-Intercalated Layered Double Hydroxides (LDHs) by Postintracrystalline Oxidation and Simultaneous Intercalation-Oxidation of Thiosulfate, Cryst. Growth Des. 12 (2012) 1378–1382. https://doi.org/10.1021/cg201452c.

[82] L. Mohapatra, K. Parida, M. Satpathy, Molybdate/Tungstate Intercalated Oxo-Bridged Zn/Y LDH for Solar Light Induced Photodegradation of Organic Pollutants, J. Phys. Chem. C. 116 (2012) 13063–13070. https://doi.org/10.1021/jp300066g.

[83] J. Zhu, H. Fan, J. Sun, S. Ai, Anion-exchange precipitation synthesis of α-Ag2WO4/Zn–Cr layered double hydroxides composite with enhanced visible-light-driven photocatalytic activity, Sep. Purif. Technol. 120 (2013) 134–140. https://doi.org/10.1016/j.seppur.2013.09.043.

[84] L.B. Staal, S.S. Charan Pushparaj, C. Forano, V. Prevot, D.B. Ravnsbæk, M. Bjerring, U.G. Nielsen, Competitive reactions during synthesis of zinc aluminum layered double hydroxides by thermal hydrolysis of urea, J. Mater. Chem. A. 5 (2017) 21795–21806. https://doi.org/10.1039/C7TA05761J.

[85] J.T. Kloprogge, L. Hickey, R.L. Frost, FT-Raman and FT-IR spectroscopic study of synthetic Mg/Zn/Al-hydrotalcites, J. Raman Spectrosc. 35 (2004) 967–974. https://doi.org/10.1002/jrs.1244.

[86] N. Touisni, F. Charmantray, V. Helaine, C. Forano, L. Hecquet, C. Mousty, Optimized immobilization of transketolase from E. coli in MgAl-layered double hydroxides, Colloid Surface B 112 (2013) 452–459. https://doi.org/10.1016/j.colsurfb.2013.07.023.

[87] K. Charradi, C. Forano, V. Prevot, D. Madern, A. Ben Haj Amara, C. Mousty, Characterization of Hemoglobin Immobilized in MgAl-Layered Double Hydroxides by the Coprecipitation Method, Langmuir. 26 (2010) 9997–10004. https://doi.org/10.1021/la1001286.

[88] Y. Feng, D. Li, Y. Wang, D.G. Evans, X. Duan, Synthesis and characterization of a UV absorbent-intercalated Zn–Al layered double hydroxide, Polym. Degrad. Stab. 91 (2006) 789–794. https://doi.org/10.1016/j.polymdegradstab.2005.06.006.

[89] J. Liu, J. Song, H. Xiao, L. Zhang, Y. Qin, D. Liu, W. Hou, N. Du, Synthesis and thermal properties of ZnAl layered double hydroxide by urea hydrolysis, Powder Technol. 253 (2014) 41–45. https://doi.org/10.1016/j.powtec.2013.11.007.

[90] M. Zouaoui, I. Jendoubi, M.F. Zid, N.F. Bourguiba, Synthesis, crystal structure and physico-chemical investigations of a new lyonsite molybdate Na0.24Ti1.44(MoO4)3, J. Solid State Chem. 300 (2021) 122221–122231. https://doi.org/10.1016/j.jssc.2021.122221.

[91] A. Mohmoud, S. Rakass, H. Oudghiri Hassani, F. Kooli, M. Abboudi, S. Ben Aoun, Iron Molybdate Fe2(MoO4)3 Nanoparticles: Efficient Sorbent for Methylene Blue Dye Removal from Aqueous Solutions, Molecules. 25 (2020) 5100–5118. https://doi.org/10.3390/molecules25215100.

[92] R.A. Nyquist, R.O. Kagel, Handbook of Infrared and Raman Spectra of Inorganic Compounds and Organic Salts: Infrared spectra of inorganic compounds (3800 – 45 cm-1), Academic Press, New York and London, 1971.

[93] M. Vafaeezadeh, M.M. Hashemi, M. Shakourian-Fard, Design of silica supported task-specific ionic liquid catalyst system for oxidation of cyclohexene to adipic acid with 30% H2O2, Catal. Commun. 26 (2012) 54–57. https://doi.org/10.1016/j.catcom.2012.04.031.

[94] K. Nakamoto, Infrared and Raman Spectra of Inorganic and Coordination Compounds: Part B: Applications in Coordination, Organometallic, and Bioinorganic Chemistry, 2008. https://doi.org/10.1002/9780470405888.

[95] G. Busca, Differentiation of mono-oxo and polyoxo and of monomeric and polymeric vanadate, molybdate and tungstate species in metal oxide catalysts by IR and Raman spectroscopy, J. Raman Spectrosc. 33 (2002) 348–358. https://doi.org/10.1002/jrs.867.

[96] T.. Basiev, A.. Sobol, Y.. Voronko, P.. Zverev, Spontaneous Raman spectroscopy of tungstate and molybdate crystals for Raman lasers, Opt. Mater. (Amst). 15 (2000) 205–216. https://doi.org/10.1016/S0925-3467(00)00037-9.

[97] J. Twu, P.K. Dutta, Raman spectroscopic studies of intercalated molybdate ions in layered metal hydroxides, Chem. Mater. 4 (1992) 398–401. https://doi.org/10.1021/cm00020a031.

[98] A.-L. Maciuca, E. Dumitriu, F. Fajula, V. Hulea, Mild oxidation of tetrahydrothiophene to sulfolane over V-, Mo- and W-containing layered double hydroxides, Appl. Catal. A Gen. 338 (2008) 1–8. https://doi.org/10.1016/j.apcata.2007.12.023.

[99] M. Rezaei, A. Najafi Chermahini, H.A. Dabbagh, Green and selective oxidation of cyclohexane over vanadium pyrophosphate supported on mesoporous KIT-6, Chem. Eng. J. 314 (2017) 515–525. https://doi.org/10.1016/j.cej.2016.12.009.

[100] F.M.P.. van Laar, D.. De Vos, F. Pierard, A. Kirsch-De Mesmaeker, L. Fiermans, P.. Jacobs, Generation of Singlet Molecular Oxygen from H2O2 with Molybdate-Exchanged Layered Double Hydroxides: Effects of Catalyst Composition and Reaction Conditions, J. Catal. 197 (2001) 139–150. https://doi.org/10.1006/jcat.2000.3070.

[101] L.J. Csányi, I. Horváth, Z.M. Galbács, Peroxide derivatives of molybdenum(VI) in neutral and alkaline media, Transit. Met. Chem. 14 (1989) 90–94. https://doi.org/10.1007/BF01040598.

[102] R. Wang, W. Jiao, B. Gao, Efficient biomimetic aerobic oxidation of phenylethane catalyzed by

P(4VP-co-St)/SiO2-supported metalloporphyrins, Appl. Surf. Sci. 255 (2009) 7766–7772. https://doi.org/10.1016/j.apsusc.2009.04.166.

[103] B. Sels, D. De Vos, M. Buntinx, F. Pierard, A. Kirsch-De Mesmaeker, P. Jacobs, Layered double hydroxides exchanged with tungstate as biomimetic catalysts for mild oxidative bromination, Nature. 400 (1999) 855–857. https://doi.org/10.1038/23674.

[104] W.Y. Hernández, F. Aliç, A. Verberckmoes, P. Van Der Voort, Tuning the acidic–basic properties by Zn-substitution in Mg–Al hydrotalcites as optimal catalysts for the aldol condensation reaction, J. Mater. Sci. 52 (2017) 628–642. https://doi.org/10.1007/s10853-016-0360-3.

[105] M. Sánchez-Cantú, L. Pérez-Díaz, E. Rubio-Rosas, V. Abril-Sandoval, J. Merino-Aguirre, F. Reyes-Cruz, L. Orea, MgZnAl hydrotalcite-like compounds preparation by a green method: effect of zinc content, Chem. Pap. 68 (2014) 638–649. https://doi.org/10.2478/s11696-013-0491-9.

[106] M.C.I. Bezen, C. Breitkopf, J.A. Lercher, On the acid–base properties of Zn–Mg–Al mixed oxides, Appl. Catal. A Gen. 399 (2011) 93–99. https://doi.org/10.1016/j.apcata.2011.03.053.

[107] T.M. Rossi, J.C. Campos, M.M.V.M. Souza, CO2 capture by Mg–Al and Zn–Al hydrotalcite-like compounds, Adsorption. 22 (2016) 151–158. https://doi.org/10.1007/s10450-015-9732-2.

[108] M. Halma, F. Wypych, S.M. Drechsel, S. Nakagaki, Synthesis, characterization and catalytic behavior of iron porphyrins immobilized in layered double hydroxides, J. Porphyr. Phthalocyanines. 6 (2002) 502–513. https://doi.org/10.1142/s1088424602000634.

[109] G.S. Machado, G.G.C. Arízaga, F. Wypych, S. Nakagaki, Immobilization of anionic metalloporphyrins on zinc hydroxide nitrate and study of an unusual catalytic activity, J. Catal. 274 (2010) 130–141. https://doi.org/10.1016/j.jcat.2010.06.012.

[110] J.R. Lindsay Smith, Y. Iamamoto, F.S. Vinhado, Oxidation of alkanes by iodosylbenzene (PhIO) catalysed by supported Mn(III) porphyrins: Activity and mechanism, J. Mol. Catal. A Chem. 252 (2006) 23–30. https://doi.org/10.1016/j.molcata.2006.01.064.

[111] K.A.D.F. Castro, S. Silva, P.M.R. Pereira, M.M.Q. Simões, M. da G.P.M.S. Neves, J.A.S. Cavaleiro, F. Wypych, J.P.C. Tomé, S. Nakagaki, Galactodendritic Porphyrinic Conjugates as New Biomimetic Catalysts for Oxidation Reactions, Inorg. Chem. 54 (2015) 4382–4393. https://doi.org/10.1021/acs.inorgchem.5b00196.

[112] W. Nam, M.H. Lim, S.-Y. Oh, J.H. Lee, H.J. Lee, S.K. Woo, C. Kim, W. Shin, Remarkable Anionic Axial Ligand Effects of Iron(III) Porphyrin Complexes on the Catalytic Oxygenations of Hydrocarbons by H2O2 and the Formation of Oxoiron(IV) Porphyrin Intermediates by m-Chloroperoxybenzoic Acid, Angew. Chemie. 39 (2000) 3646–3649. https://doi.org/10.1002/1521-3773(20001016)39:20<3646::AID-ANIE3646>3.0.CO;2-Q.